Understanding the Development of Cam-Type Deformity by FE Analysis of the Immature Proximal Femur

Pauline Roels

Master Thesis

Supervisor: Dr. Ir. A.A. Zadpoor
Professor: Prof. Dr.Ir. H.H. Weinans

Delft University of Technology
Department Biomedical Engineering
Tissue Biomechanics and Implants

June 12, 2013

ACKNOWLEDGEMENTS

I would like to thank my supervisors Dr. A.A. Zadpoor who is working hard to expand the tissue biomechanics group. The arrangement of the computational lab and organized group lunches and meetings, made the whole working atmosphere much more pleasant. Additionally, I would like to thank him that he ensured that I proceeded in the right direction and that he was always approachable for questions. I would like to thank Prof.dr.ir. H.H. Weinans for his supervision. His knowledge on the topic helped me a lot during project and to approach the results. Furthermore, I would like to thank doctoral student R. Agricola for providing the data set which made the whole project possible and for introducing me to the topic and always being enthusiastic. Finally, I would like to thank doctoral student Gianni Campoli who devoted a lot of time assisting me with the FE modeling in Abaqus.

ABSTRACT

Cam impingement appears to be an important factor in the development of early osteoarthritis (OA) of the hip. A Cam is generally diagnosed in young and active adults, already at the age of thirteen. Therefore, it has been suggested that excessive femoral loading during skeletal development might trigger the abnormal morphology. The goal of this research is to understand how the deformity develops. A finite element analysis is conducted to predict the stress distribution in the immature proximal femur under different loading conditions. Furthermore, the influence of the orientation of the epiphyseal plate is studied, as a Cam-type deformity is highly associated with an abnormal epiphyseal extension on the anterosuperior region. Previous studies suggested that octahedral shear stress promotes growth, while hydrostatic compressive stress inhibits growth. These mechanobiological principals are implemented to predict the bone growth rate.

The position and the shape of the growth plate, as well as the loading direction highly influence the stress distribution in the proximal femur and growth plate. A medial directed load causes high compression stress in the growth cartilage in the lateral region. Endochondral growth is inhibited, which could result in a deflection of the growth plate, observed in Cam patients as epiphyseal extension. High regional stresses and osteogenic index appear in the epiphysis at the anterosuperior region when a convex growth plate is modeled. These results would support the theory that a Cam-type deformity might not be a result of endochondral growth, but the higher stresses demand local remodeling and apposition.

Incorporating dynamic loading and tissue adaptation is needed to further understand how mechanical stimuli effects the epiphyseal growth and to predict morphological changes over time. Once one understands the etiological factors of cam impingement, the disorder can be treated at an early stage and the development into early osteoarthritis might be prevented.

TABLE OF CONTENT

1. INTRODUCTION

In cam femoroacetabular impingement (FAI), an osseous bump at the femoral head neck junction results in an abnormal contact between the acetabulum and femoral head during motion. This morphological abnormality is shown in Fig 1. The impingement causes higher compression and shear forces in the hip joint that will damage the adjacent articular cartilage and labrum if left untreated (1). Therefore, cam impingement is thought to be an important factor in the development of early osteoarthritis (OA) of the hip, especially in young and active adults (2-6). For this reason, there has been an increasing interest in this topic during the last decade. A lot of studies focus on improving the diagnosis options (7-10), characterizing the related symptoms (11, 12) and identifying the best treatments possibilities (13-16). Nevertheless, the etiology of cam impingement is not yet well understood. This research focuses on understanding the development of the cam-type deformation.

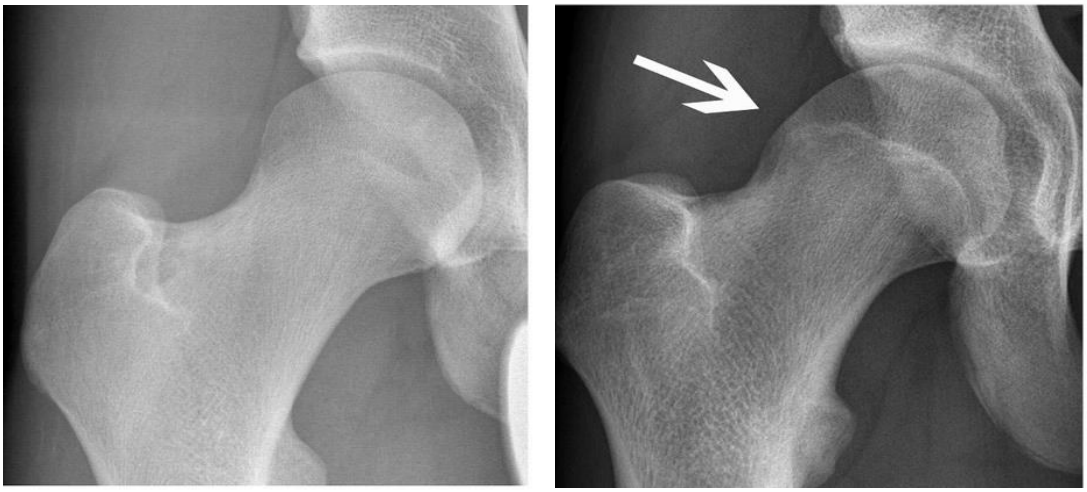

a) **b)**

Fig. 1 *Two anteroposterior radiographs of (a) a normal femur with a convex structure and (b) a femur with a prominence bump at the femoral head neck junction. Adopted from Agricola et al. (17).*

The formation of the osseous bump that causes the impingement might be due to femoral disorders such as slipped capital femoral epiphysis (SCFE) (18-20), Legg-Calve-Perthes disease (21), or other endocrine or metabolic disorders (22, 23). Additionally, incorrect healing after fracture can result in a bump at the anterosuperior region (24, 25). However, cam-type deformity is observed even when there is no sign of pediatric diseases or former fracture. As cams are generally diagnosed in young and active adults (17, 26-28), it has been suggested that excessive femoral loading (due to a high level of physical activity during skeletal development) might also trigger the abnormal physeal morphology

(29). Agricola et al. (17) studied the pre-professional soccer players of Feyenoord and compared them with a control group of the same age (12 to 18 years). They observed a significant larger prevalence of a cam-type deformity in the athletes group. Furthermore, both the flattening and prominence bump are already present at the age of 13, before complete closure of the epiphyseal plate. The prevalence increases with age that suggests that cam deformation develops during adolescence. Similar trends were observed by Siebenrock et al. (26). In addition, both Agricola and Siebenrock et al. (30) observed that cam-type deformity is associated with a more horizontally orientated epiphyseal plate. This orientation results in an abnormal extension on the anterosuperior side, which makes the head neck junction less concave (31). Therefore, both the loading scenarios and orientation of the epiphyseal plate might influence the development of cams. The extension of the epiphysis can be the result of a delayed separation of the greater trochanter and the femoral head or higher stresses on the growth plate require a structural adaptation. Sports that require, an extreme range of motion (ROM), for instance kicking or jumping, coupled with the downwards compression of body weight, will increase the contact of the femoral head and acetabulum leading to higher mechanical stresses in the femur. Chronic mechanical stress has a great impact on the structure and tissue properties of bone during skeletal development (32). Immature skeletons are especially more responsive to mechanical loading, because their tissue is more elastic and the remodeling process is more active (33). The epiphysis is a vulnerable region of the bone, since the tissue properties of the growth plate differ from the surrounding trabecular bone. A local distortion in this region could influence the general shape and internal structure during the development of the proximal femur (34). A repetitive trauma caused by high levels of physical activities could also widen the epiphyseal plate making it more vulnerable to trauma (33).

Further understanding of how mechanical stimuli affect the physeal growth is needed to comprehend all the physical and physiological aspects. Unfortunately, prospective longitudinal studies require a long-term follow-up and a proper control study group, that is time consuming and can raise ethical questions as a consequence of the radiation exposure on young healthy joints. Moreover, in such studies it is difficult to find a causal relation, as intervening factors cannot be easily excluded. Finite element analysis (FEA) can be very useful to predict morphological changes over time and is used

frequently to analyze the mechanical behavior of bone (35, 36). Previous FE studies focus on how cam-type impingement influences the contact stresses in the hip joint (37-39). The stress and strain distribution patterns on the subchondral bone and articular cartilage are analyzed to establish if cam impingement could lead to early osteoarthritis. Furthermore, the effect of osteochondroplasty on the stress distribution in the femoral head is evaluated by Alonso-Rasgado et al. (40). Several studies confirm that femoral osteochondroplasty can restore the range of motion, provide a quick pain relief and might decelerate the degeneration of the hip. However, the latter remains unclear due to a lack of long term results. Additionally, Patients will benefit most when the surgical intervention is performed at an early stage (41, 42). However, to the best of author's knowledge, there are no FE studies that consider mechanobiological principles to investigate the development of the deformity itself. Once one understands the etiological factors of cam impingement, the disorder can be treated at an early stage and the development into early osteoarthritis might be prevented.

The aim of this paper is to create a three-dimensional FE model of an immature femur to investigate how the orientation of the epiphyseal plate combined with different loading directions will influence the stress and strain distribution in the proximal femur.

2. METHODOLOGY

The finite element model generation consist of three basic steps:

1. Geometry acquisition
2. Meshing of the model
3. Constitutive modeling of the material

By using the CT scans of young and healthy adolescents, one can non-invasively retain the 3D geometry and material properties and create an FE Model of the proximal femur. Subsequently, different load magnitudes and directions can be applied to simulate normal and extreme loading after which simulations are performed. The whole procedure is extensively described in this chapter. Since the growth plate orientation will be used as an input parameter, the epiphyseal extension is determined first.

2.1 Medical Image Analysis

To understand if and how the orientation of the growth plate is involved in the development of cam-type impingement, extra morphological measurements on the dataset of the study group of Agricola et al.(17) were conducted. Sixty three baseline anteroposterior (AP) pelvic view radiographs of the pre-professional soccer players that were cross checked during a follow-up were used for this purpose. To examine the femoral shape differences and quantify the epiphyseal extension onto the femoral neck, landmark based registration was performed. This was done by using the *cpselect* tool from the image processing toolbox in Matlab (R2011b), where 45 corresponding landmarks were placed on two images at the same time for all the scans. The growth plate was annotated by an upper and lower line. An example can be seen in Fig 2.

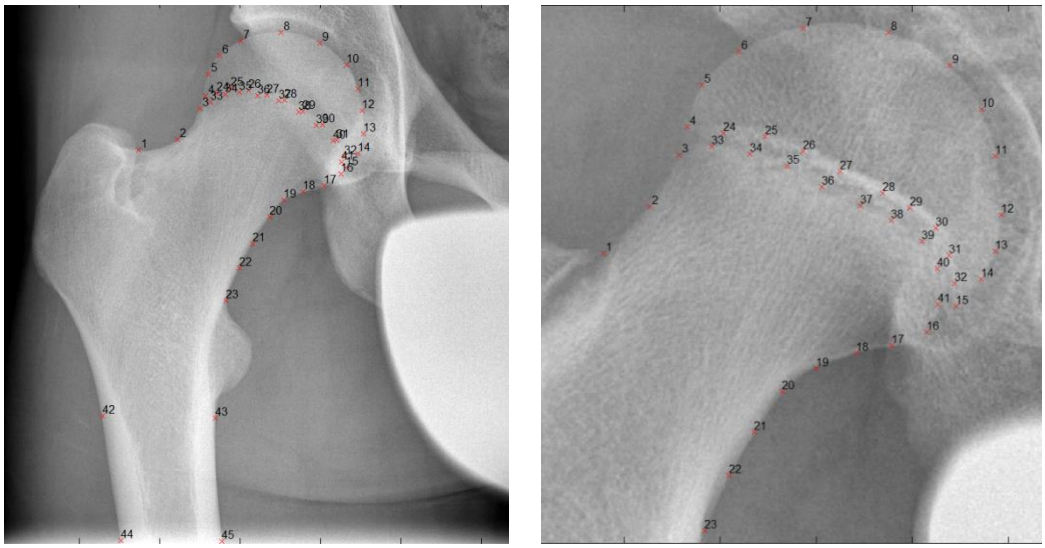

a) **b)**

Fig. 2 *Positioning of the 45 landmarks on the radiographs using Matlab (a) and a close up to visualize the landmarks indicating the growth plate (b). The morphological measurements on Figure 4 are based on these coordinates.*

The points were exported to the workspace, where they were saved as 45x2 matrices containing the x- and y-coordinates of the landmarks. Based on these landmarks the neck-shaft angle and growth plate orientation was measured. So far, there is no standardized method to measure the physeal orientation. Therefore, the tilt angle (Fig. 3b) (43) and the epiphyseal extension (Fig. 3c) as described by Siebenrock et al. (31) were chosen. The tilt angle is defined by the line that runs through the superior and inferior endpoint of the growth plate and the tangent where the neck axis intersects with the best

fitting circle around the femoral head. The Kasa method was used for the simple algebraic circle fit (44). The landmarks 5 and 6 on the femoral head were excluded in the fitting procedure, because the femoral head appears more oval if the growth plate is still open anterosuperiorly (17). The epiphyseal extension is the distance between the superior and inferior endpoint of the growth plate and the tangent, divided by the head radius (Q1/ Q2), respectively. Additionally, two circles were fitted through the upper and lower landmarks that annotate the growth plate. The distance to the neck axis represents the extension in the neck and the radius of the circle determines the roundness of the physis, Fig. 3d. Both the left and right femurs were considered, since the affected site is independent of leg dominance. To determine the differences in extension between the Cam and no Cam group a Student's t-test was used. Positioning of the landmarks is essential for these measurements. The inter- and intra-observer variability was tested in 10 randomly selected radiographs for 6 measurements with an interval of 2 months. The intra-class correlation coefficient (ICC) was used to validate the landmark positioning.

2.2 FE Model

Model Geometry

The geometry of the femur was extracted from a CT data set of a young and healthy hip joint using the image processing software Mimics software 14.0 (Materialise N.V., Belgium). The CT-scans came from a database of the Erasmus Medical Centre, Rotterdam and were conducted using Siemens Emotion6 with the following parameters: 110kV peak, 39 mA, a pixel size of 0.545mm and a slice thickness of 1.3 mm. That is thin enough to account for the complex innominate structure (45). The subject information is presented in Appendix1. The DICOM images were imported in Mimics after which thresholding and region growing operations were performed to segment the femoral bone tissue of the left femur. Furthermore, visual segmentation at each slice and morphological filters were applied to reduce non-smooth surfaces of the femur.

A convergence study was conducted to find the optimal type and number of elements considering the computational time and accuracy of the results. Both 10-node quadratic tetrahedral elements (C3D10) and 4-node linear elements (C3D4) were used for this purpose. The averaged edge length, number of elements and number of degrees of freedom (NDOF) are presented in Appendix 2. For this study the

femur was modeled without a growth plate and with isotropic, linear elastic, homogeneous material, because a density based relation will make the material properties mesh dependent that will influences the outcome. The Young's modulus of the bone was set to 6000MPa with a Poisson's ratio of 0.3. The magnitudes should not influence the outcome, but for completeness they were chosen within the normal physiological range (46). A concentrated force of 1200N (2.5 times Body Weight) was applied on the center of the femoral head, which represents the resultant hip contact force during normal walking (47).

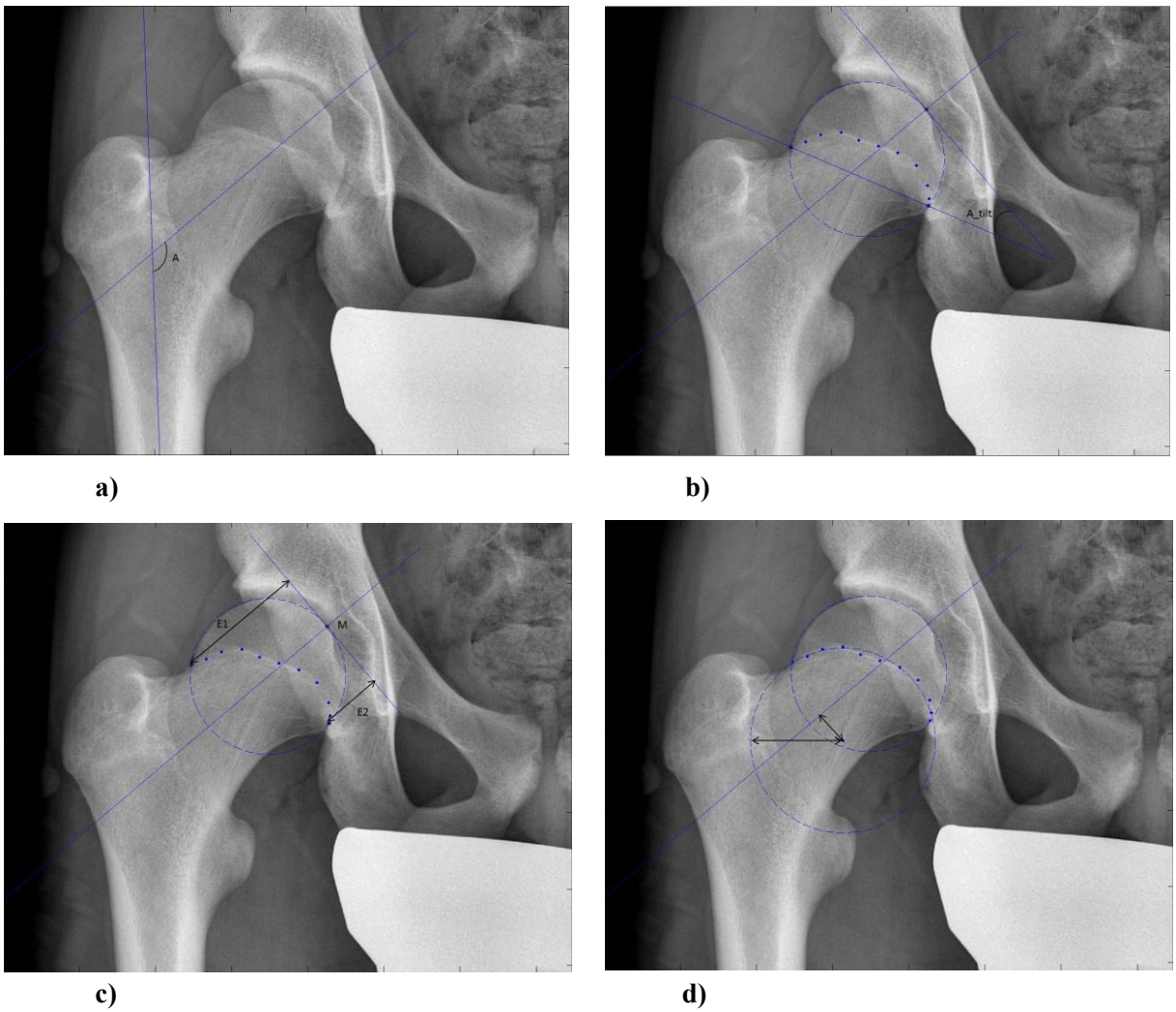

Fig. 3 *The morphological measurements; (a) Neck-shaft angle, (b) Tilt angle, (c) Epiphyseal extension of the superior (E1) and inferior (E2) endpoint of the growth plate. The values are divided by the head radius to calculate Q1 and Q2, respectively, (d) The radius and the distance of the midpoint to the neck axis of the circle that characterizes the shape and orientation of the growth plate.*

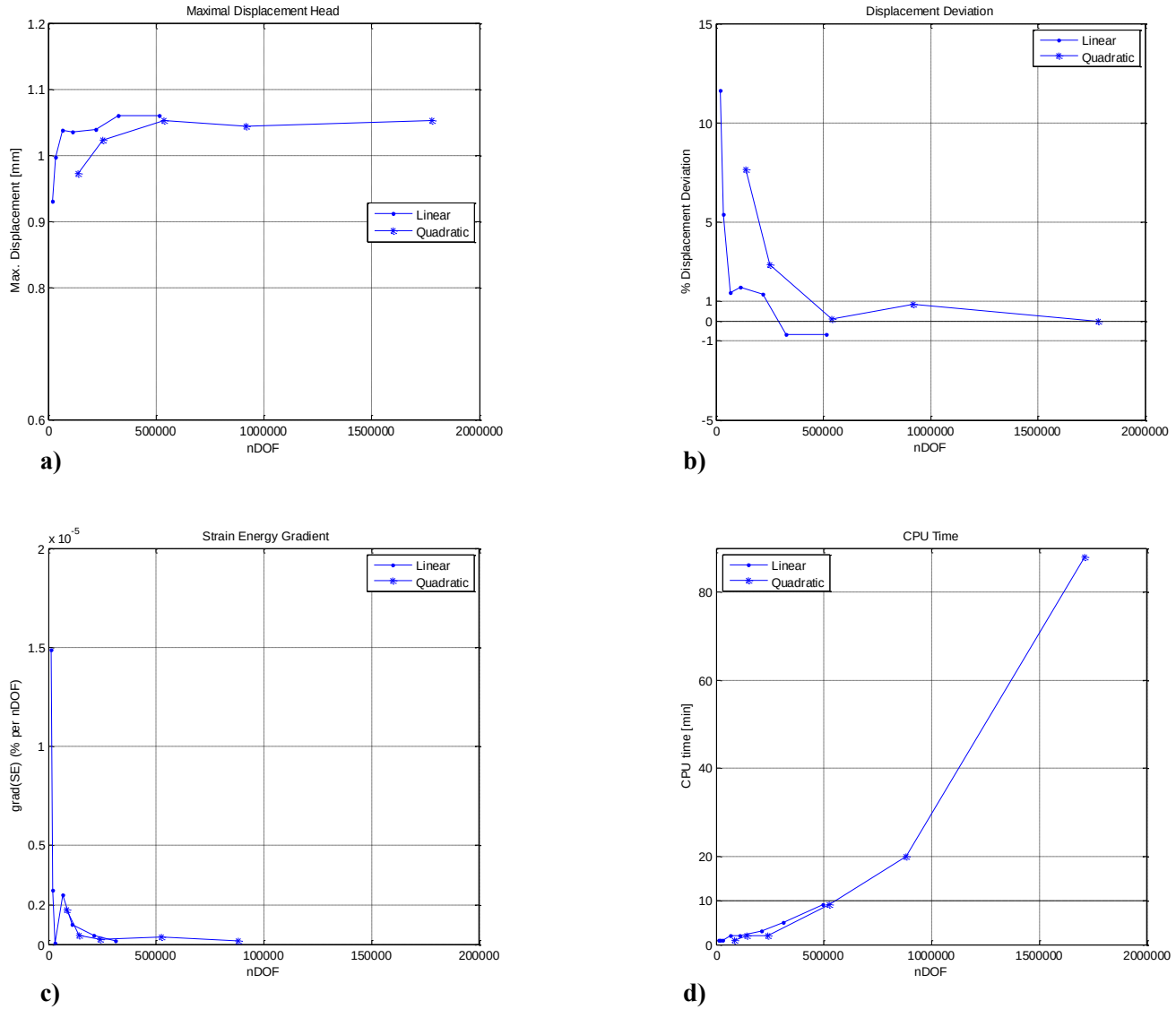

Fig. 4 *The maximal displacement of the femoral head (mm)(a), the displacement error (%)(b), the strain energy gradient; grad (SE)(c)and the central processing unit (CPU) time (min) (d) are plotted against the number of degrees of freedom (NDOF) for the 7 linear and 5 quadratic models.*

The maximum displacement u^{max} and displacement deviation u^{dev} were calculated in a region on the femoral head that is not directly influenced by the external force or the growth plate. As the number of elements increases, the results should converge to the correct solution and the deviation to zero.

$$u^{dev} = \frac{u^{ref} - u^{i}}{u^{ref}} \cdot 100\ (\%) \quad (1)$$

u^{ref} represents the maximum displacement of the model with the highest NDOF. u^{i} is the maximum displacement in the ith mesh refinement. Furthermore, the strain energy gradient $grad(SE)$ was considered (48);

$$grad(SE) = \frac{(SE^{i+1} - SE^{i})/SE^{i}}{NDOF^{i+1} - NDOF^{i}} \cdot 100\ (\%) \quad (2)$$

SE^{i} represents the total strain energy of the model in the ith mesh refinement. For an elastic body, the strain energy of the system is equal to the work done by the external forces. By increasing the mesh refinement the discretization error decreases, the SE will converge and the grad(SE) will reach zero. The results are depicted in Fig 4. Although quadratic elements showed a better performance as they can more accurately represent curved surfaces, the finest linear element mesh was chosen. For realistic modeling of the growth plate, which has a thickness of around 2-3mm, the element size cannot exceed these values. In Fig. 4a and b the maximal displacement and displacement deviation are presented, respectively. The finest linear mesh, with an averaged edge length of 0.93mm, gave a displacement deviation of less that 1%, while the computational (CPU) time was still within 10 minutes (Fig. 4d). Decent results were also found for the strain energy gradient, Fig. 4c. The absolute value of the normalized total strain energy gradient dropped under $0.2 \cdot 10^{-5}$ (% per NDOF), which represents less than 1% deviation in total SE. The meshing protocol was performed in 3-matic (Materialise N.V., Belgium), then the model was exported back to Mimics to assign the material properties. The parameters used for the segmentation and meshing protocol are presented in Appendix 3.

Material Properties

The material properties of the model were based on the Hounsfield Unit's (HU) derived from the CT scans. In Mimics the average HU value for each element is computed and 200 bone density values were assigned according to the following linear relation;

$$\rho\ (\mathrm{g/cm^3}) = \alpha + \beta HU \tag{3}$$

Since there was no calibration phantom included in the scan, the α and β were determined based on the HU value of air (-1024) and the mean HU value of the cortical bone (1016.04) derived from the scans. A cortical bone mask used to determine this value had a threshold value of 700 HU (49). As depicted in Fig. 5, the mask segments mainly the shaft. The head and neck of the undeveloped femur consist mainly of trabecular tissue; therefore the HU threshold value of 700 is acceptable. The air density was set to 1.225e-3g/cm³. A cortical bone density of 0.9g/cm³ was chosen (50), resulting in α=0.45 and β=0.44e-3. A mean HU-ρ relation which can be used when there is no phantom present (51) gave higher density values, therefore was rejected.

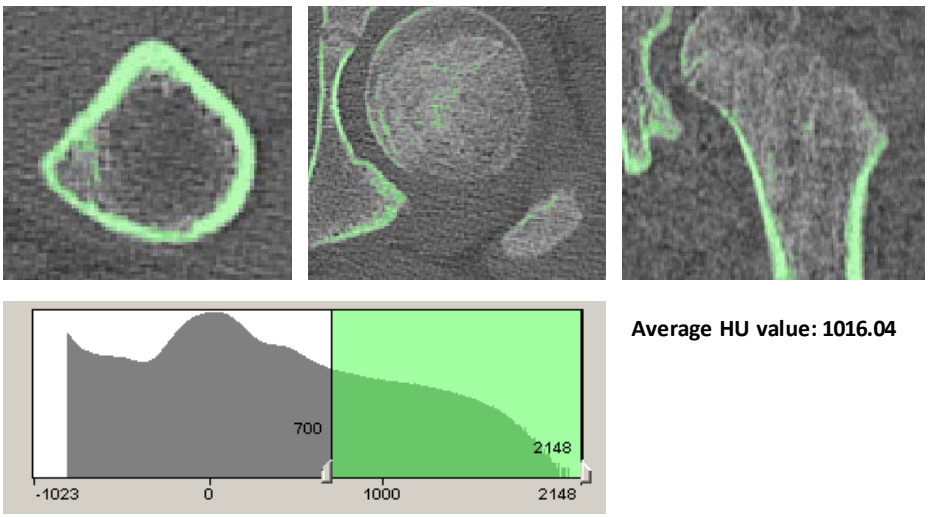

Fig. 5 *Three radiographic slices indicate the cortical bone mask threshold region (green), ranging from HU=700-2148. The average HU value of the cortical bone mask is 1016.04.*

For quantifying the local bone stiffness the relation between the bone density and Young's modulus of cortical bone needs to be considered. Numerous studies describe the mathematical relation between the mineral bone density and the Young's modulus (52), however all are based on experimental data of adult bone. Öhman et al (50) tested the cortical bone tissue of children. Since the mean density value of that paper was used to determine constants in equation 3, their power law relationship was used;

$$E(MPa) = 12900 \cdot \rho^2 \tag{4}$$

A resulting average cortical bone modulus of 17 GPa was a bit high for young bone. Berteau et al (46) and Taddei et al (53) found lower values, 9.1 GPa and 14.5 GPa, respectively. However, most of the model consisted of trabecular bone with a mean value of 4 GPa, as depicted in Appendix 4. Consequently, Öhman's density stiffness relation was used together with a poison's ratio of 0.3 (54). The growth plate was modeled with a constant Young's modulus of 6 MPa and a Poisson's ratio of v=0.49, to account for almost incompressible material (55). All materials in the model had isotropic, linear elastic properties, which is commonly used is FE studies of the proximal femur (49, 56). It is found by Peng et al (57) that there is a small difference in mechanical responds in isotropic and orthotropic material. Especially, when using an heterogeneous material model (58). The viscoelastic properties of the growth plate were not considered since the analysis did not involve cyclic loading (59). After the constitutive modeling of the material, the model was imported into Abaqus 6.10-1 FE Analysis Software (Dassault Systemes Simulia) for further analysis. The entire segmentation, meshing and material assignment protocol is illustrated in Fig 6.

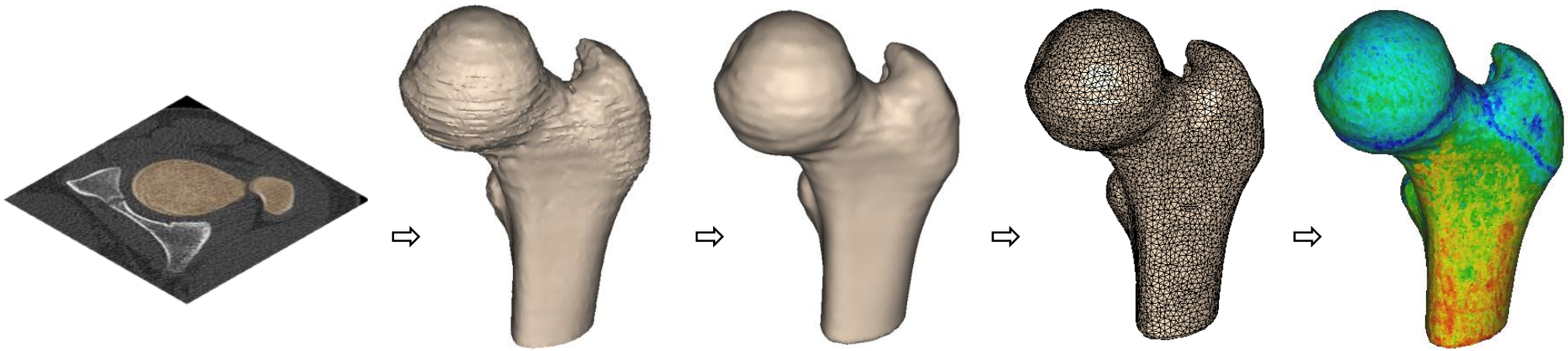

a) **b)** **c)** **d)** **e)**

Fig. 6 *This figure illustrates the algorithm generating a finite element (FE) model. Staring with (a) Bone segmentation on 2D DICOM images (b) Creation of a 3D surface (c) Smoothing of the surface (d) Volume mesh generation e) Applying material properties based on density values of the CT images.*

Growth Plate Segmentation

The measured epiphyseal extension does not describe the shape of the growth plate, therefore, both flat and convex plates were modeled. In Appendix 5 the orientation procedure is illustrated. The model was positioned in such a manner that it corresponds to the AP pelvic view. A cross-section was created to draw the neck axis and tangent line to determine superior and inferior extension, point A and B, respectively. The actual epiphyseal extension values that were used are presented in the first part of the results in the medical image analysis. The convexity of the growth plate was based on visual analyses of the CT scans. An average growth plate length-height ratio of 6:1 resulted in a height of around 6.7mm (Point C). Points A, B and C were used to determine the coordinates of the midpoint of the sphere (D) that annotates the convex shape. The radii, r1 and r2, had a difference of 3 mm, corresponding to a growth plate thickness of a 12 year old. The flat growth plates were modeled using two cylinders with midpoints D1 and D2 with the same orientation as the convex plate. The distance between D1 and D2 described the thickness of the growth plate. The coordinates and radii of the spheres and cylinders used are presented in Appendix 6.

A comparison study was conducted in segmentation of the growth plate before and after the model was meshed, using Mimics and Abaqus respectively. In Abaqus, the elements that represent the growth plate were selected using the function *getByBoundingSphere* in a Phyton script. This function creates a set of elements where the femur intersects with the sphere. By subtracting two spheres with the same origin and different radius, the convex growth plate was segmented. A comparable method was used for the flat growth plate, using *getByBoundingCylinder*. Afterwards, the material properties were assigned to the growth plate section. The segmenting of the growth plate in Mimics was done before creating the mesh. Spherical and cylindrical masks were created using CAD tools. These masks were modified using Boolean and morphological operations to create a growth plate surface, which fell inside the femoral surface. The two surfaces were exported in 3-matic and merged before creating the volume mesh. Unfortunately, the surface of the growth plate could not intersect with the outer femoral surface, leading to a small gap between the growth plate and the femur. These elements were added to the growth plate section in Abaqus later on, using the same scripts *getByBoundingSphere* and *getByBoundingCylinde.*. The trochanteric growth plate, which was included in one of the models, was

also segmented in Mimics based on its visual features. In Appendices 7-9 the Abaqus and Mimics segmentation protocol is illustrated, including the differences in surface structure.

Loading Conditions

In this study various hypothetical loading conditions were analyzed. The literature was consulted to find suitable force magnitudes and inclination angles. The first 'control' loading scenario was based on the resultant hip contact force of the normal walking cycle of the study of Bergmann et al. (47). Although the number of patients in that study is limited and they do not represent the general population as they already have an implant, the results give a global indication of the magnitude and direction of the hip contact force. A peak force of 1200N was applied, 250% body weight (BW) with an inclination angle of 15º and 35º in the coronal and transverse plane, respectively. Since nothing is stated on the angle in the sagittal plane, the value of 20º was used, based on the normal gait cycle in the study of Carriero et al (60).

So far, it is not clear what types of movements are involved in the developed of a Cam deformity or even if they are involved. A 90 degrees of flexion in combination with internal rotation causes the impingement of the femoral neck against the acetabulum. Therefore, it is suggested that these motions might also influence the development. Carriero et al. studied the gait cycle of children with Cerebral Palsy (CP), which have muscle spasticity that results in excessive internal hip rotation. Based on this study an inclination angle of 40º in the coronal plane in loading case 2 was chosen, which reflects an internal rotation. In case 3 the load was placed on the position where the Cam deformity would appear, 15º lateral in the anterosuperior region. For case 4, different motions were analysed from the Orthoload database for movements that correspond to an extreme hip flexion (61), depicted in Appendix 10. An inclination angle of 80º in the transverse view corresponded to a pronounce hip flexion. An overview of the inclination angles of the four loading cases is presented in Fig. 7.

In the study of Carter et al. (62) they used a reduced force magnitude for the extreme range of motion cases. However, several papers found higher force magnitudes as 550% BW for movements like running (63) and jumping/push jerking (64) and 450% BW in alternating jumping (61). This study focused on the stress and strain distribution rather than the exact values. For that reason, the force magnitude of 250% BW was used in all loading scenarios for objective comparison between the

angles of inclination. All joint reaction forces were applied as pressures and distributed over a circular path with a 15mm diameter.

Additionally, the loading scenario 2 and 3 were extended with the implementation of a muscle force. The abductor muscles that attach to the major trochanter play an important role in the development of the lateral part of the femur (65). To understand how these muscle forces influence the stress distribution, a tensile force was added with and without modeling of the trochanteric growth plate. The inclination angles were obtained from the second and third load case of the study of Carter et al. (62) (62), as their contact force directions correspond to the directions in Case 2 and 3. The tensile force was applied as a traction force over an area of 155mm² with an inclination angle of 35º and -8º for Case 2 and 3, respectively. The magnitude of the muscle force was 364 N, 3.3 times lower than the hip contact force (62). In Appendix 11 an overview is given of all the magnitudes and angles of inclination of the loading scenarios. In all loading cases the distal end of the femur was fully constrained.

Analysis

Longitudinal bone growth is the result of interstitial expansion followed by endochondral ossification at the epiphyseal growth plate (33). During adolescence the whole cartilage region is replaced by bone, the growth plate closes and the longitudinal bone growth stops. Beside hormone and growth factors, mechanical loading directly affect endochondral bone growth and ossification (22, 66). According to Hueter-Volkmann's law, pressure on the epiphyseal plate retards bone growth, while tension accelerates it (66, 67). This principle can be simulated using analytical mechanobiological models of Stokes (68) and Carter (69). In the Stokes's model, the axial stresses with respect to a homeostatic condition are used to determine the longitudinal strain increment which is added to the baseline growth to calculate the growth strain increment. In this analysis the mechanobiological model of Carter was used to predict bone growth. This model takes three dimensional stress stimuli into account that occur in a complex mechanical environment, while Stokes only incorporates axial stresses (66).

Carter (1984) was one of the first to propose a theoretical framework for mechanobiology of skeletal development (70). The mechanobiological model was developed to simulate bone growth in which the growth rate is described as the change in length which has a biological and mechanical component (71).

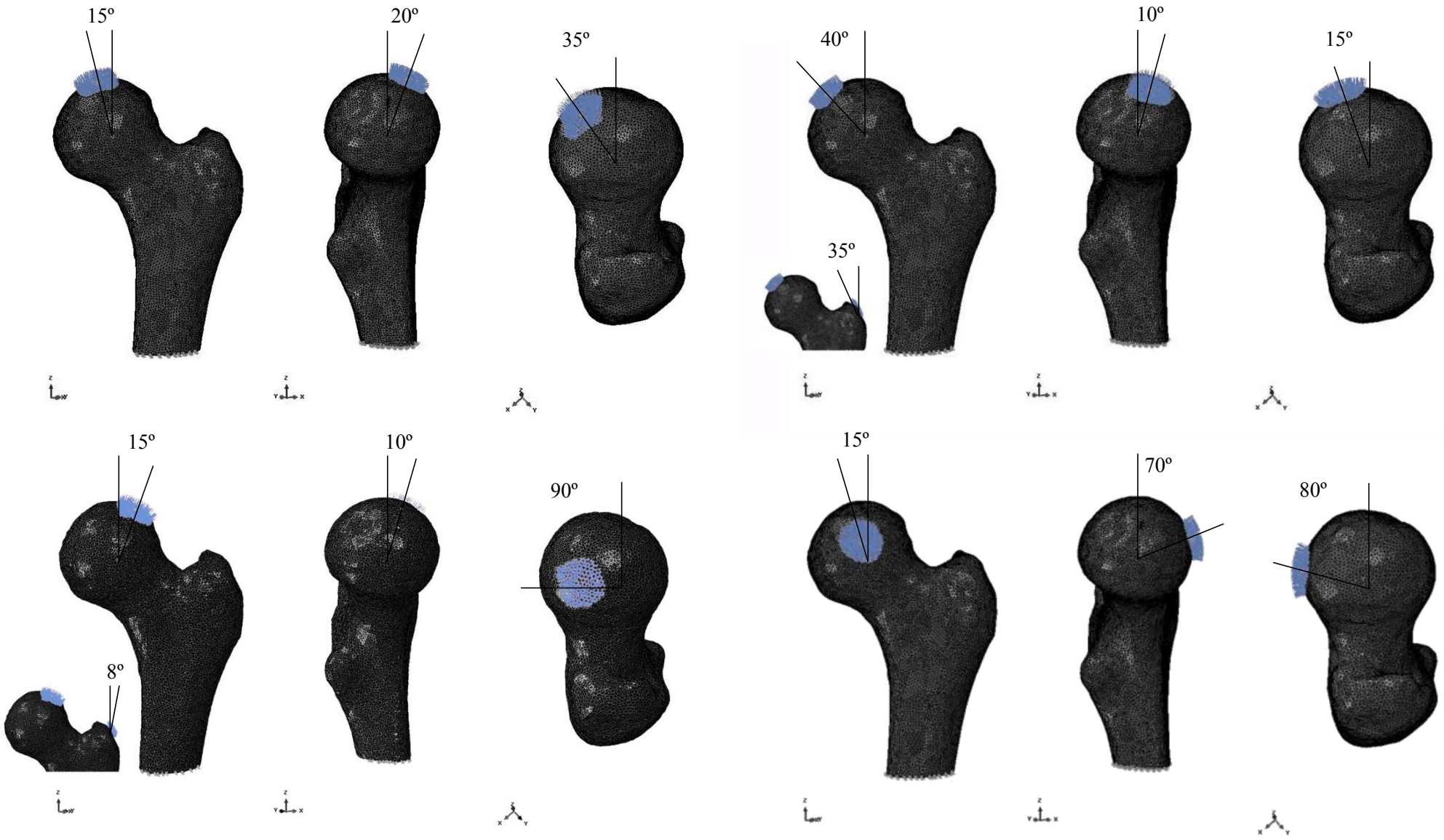

***Fig.** 7 Four loading cases presented in the coronal, sagittal and transverse view. Loading scenarios 2 and 3 are extended with the implementation of a muscle force of 364N. The hip contact force magnitude is 1200N.*

Bone growth is mostly affected by biological factors which are depending on intrinsic genetic factors, hormonal regulation and nutrients. The biological component is usually set as a constant, when studying the mechanical influence on the growth rate. The mechanical factors are essential in early development, their effect reduces when reaching skeletal maturity (72). The mechanical component can be described by the osteogenic index (OI) introduced by Carter and Wong (69);

$$\dot{\varepsilon}_m = OI = a \cdot \max(\sigma_{Si}) + b \cdot \min(\sigma_{Hi}) \quad (5)$$

Carter et al. (70) states that cyclic hydrostatic stress inhibits bone growth, while cyclic octahedral shear stress stimulates growth. The constants *a* and *b* determine the influence both components have on the growth rate. Bone grows between 40-80% of the normal size without mechanical loading. The ratio b/a should be set between 0.3and 1, for a mechanical contribution that is half the biological contribution, to model accurate endochondral ossification. In this study the biological component was not included and *b* was set to 0.5 (73, 74). The distribution of the octahedral shear stress, hydrostatic compression stress and growth indexes was plotted for the growth plate and an axial cross section of the femur. Additionally, the strain distribution was plotted. The analysis was performed in Abaqus (version 6.10-1) FE Analysis Software.

3. RESULTS

3.1 Medical Image Analysis

When comparing the radii of the circles that annotated the upper and lower line of the growth plate with the flattening of the growth plate visually in the scans, no clear relation was found. This also applies to the distance of the midpoint of the circle to the femoral neck axis compared to the extension in the neck. For this reason, mean vales of the tilt angle and the epiphyseal extension Q1 and Q2 are presented in Appendix 12 as the results of the medical image analysis. The mean values of the neck-shaft angle, tilt angle, Q1 and Q2 are calculated for the groups with and without a Cam, for an open and closed growth plate. One of the parameters used in radiographic tests to quantify a Cam deformity is the alpha angle (AA) introduced by Nötzli et al. (8). The alpha angle is the angle between the neck axis and the line from the center of the femoral head through the point where the cortical surface

exceeds the radius of a perfect circle drawn around an ideally spherical femoral head. An angle higher than 60 indicates a Cam. Furthermore, a three point scoring system can be used to identify a Cam. The highest hip (HH) score 1 indicates a normal joint, 2, a flattening of the head-neck junction and 3 a prominence bump (17). These quantifications are performed on the baseline and follow-up scans by Agricola et al. (17)(new paper Agricola).

Higher Q1 values are found in the Cam group for both quantification methods, HH score ($p=0.047$) and the AA score ($p=0.001$). This hold for both an open and closed growth plate. However, when considering the follow up CT scans, Q1 was not a predicting factor in the development of a Cam (new paper Agricola). There was no statistical difference for the Q2 values of the Cam group (HH: $p=0.056$ and AA: $p=0.845$). Whereas the tilt angle, only shows significant higher values ($p=0.024$) when considering the open growth plates and the Cam group is determined by the alpha angle. When evaluating all hip a positive correlation was observed between the alpha angle and epiphyseal extension (Q1). The correlation coefficient was 0.74($p<0.001$). Therefore, the mean measured epiphyseal extension (Q1) was used as the input for the growth plate orientation (A=1.6 and A=1.4). Since the difference in orientation was minor an extra growth plate was modeled almost perpendicular to the neck axis (A=1.2). The mean Q2 value was used to determine the inferior extension for all growth plates (B=0.9), as there was no statistical difference between the Cam and no Cam group. These results led to 3 growth plate orientation for both the flat and convex shape (GP1, GP2 and GP3), the latter being to most horizontal. The coordinates and radii of the spheres and cylinders used to annotated the convex and flat growth plates are presented in Appendix 6. Furthermore, a lower neck-shaft angle was found in the Cam group with an open growth plate, considering at the alpha angle ($p<0.001$), however, it was not possible to parameterize this in the model. The neck-shaft angle seems to increase after epiphyseal closure, while in the group without a cam the angle decreases. The intra-class correlation coefficient (ICC) to validate the landmark positioning gave a score of 0.97 (intra-observer) and 0.97 (inter-observer) reliability for the epiphyseal extension (Q1).

3.2 FE Analysis

Abaqus vs. Mimics Segmentation

The hydrostatic stress plots in Fig.8 and 9 show similar but much smoother distributions when the segmentation is performed in Mimics. This also holds for the octahedral shear stress and osteogenic index distribution. The magnitude of the hydrostatic stress in the different plots corresponds well. This is not true for the shear stress and strain magnitude, which is lower when the segmentation is performed in Abaqus, Fig. 10. Consequently, the OI magnitude is slightly lower as well. The high and low stress peaks on the edge of the growth plate when the segmentation is performed in Mimics are not seen in the Abaqus segmentation plots.

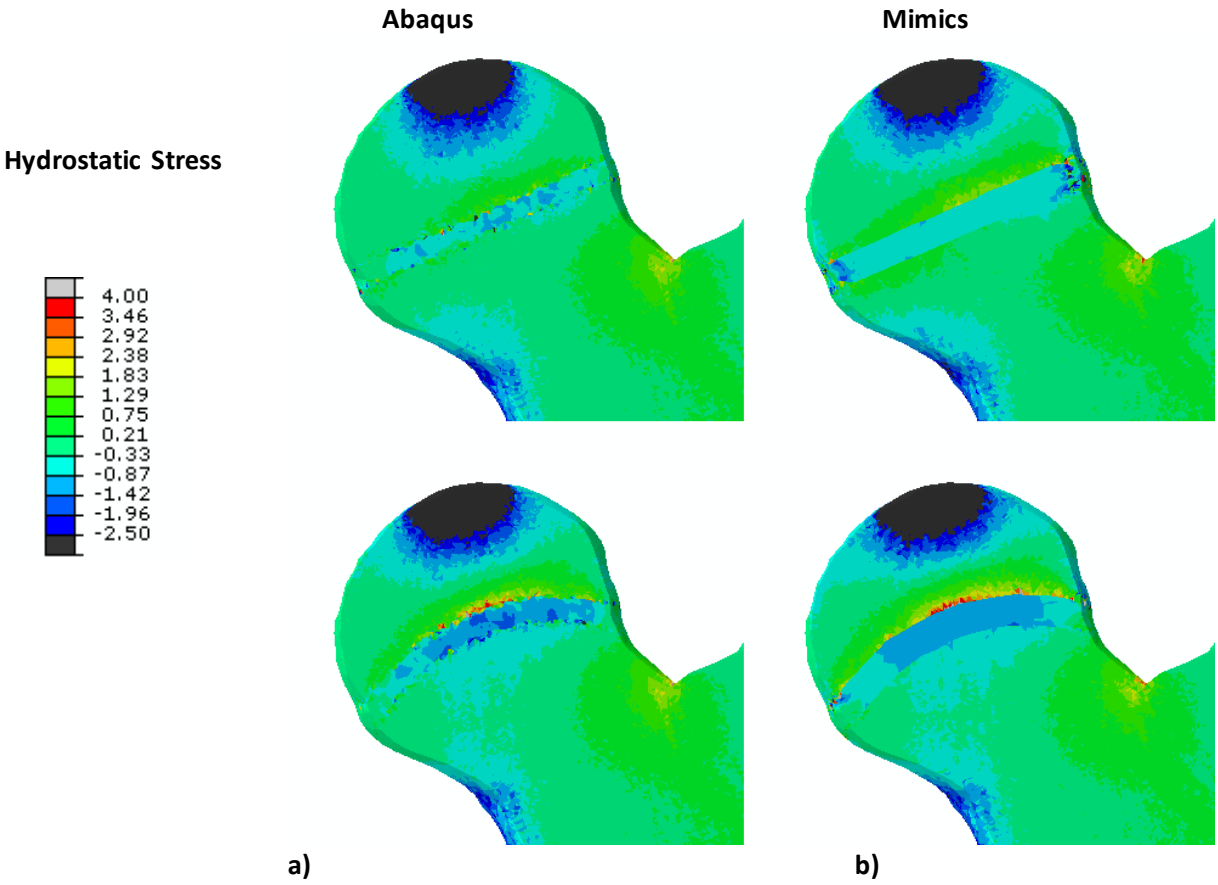

Fig. 8 *Hydrostatic Stress plots of femoral head-neck region with a flat and convex growth plate (GP2) segmented in Abaqus (a) and Mimic (b) under loading case 1.*

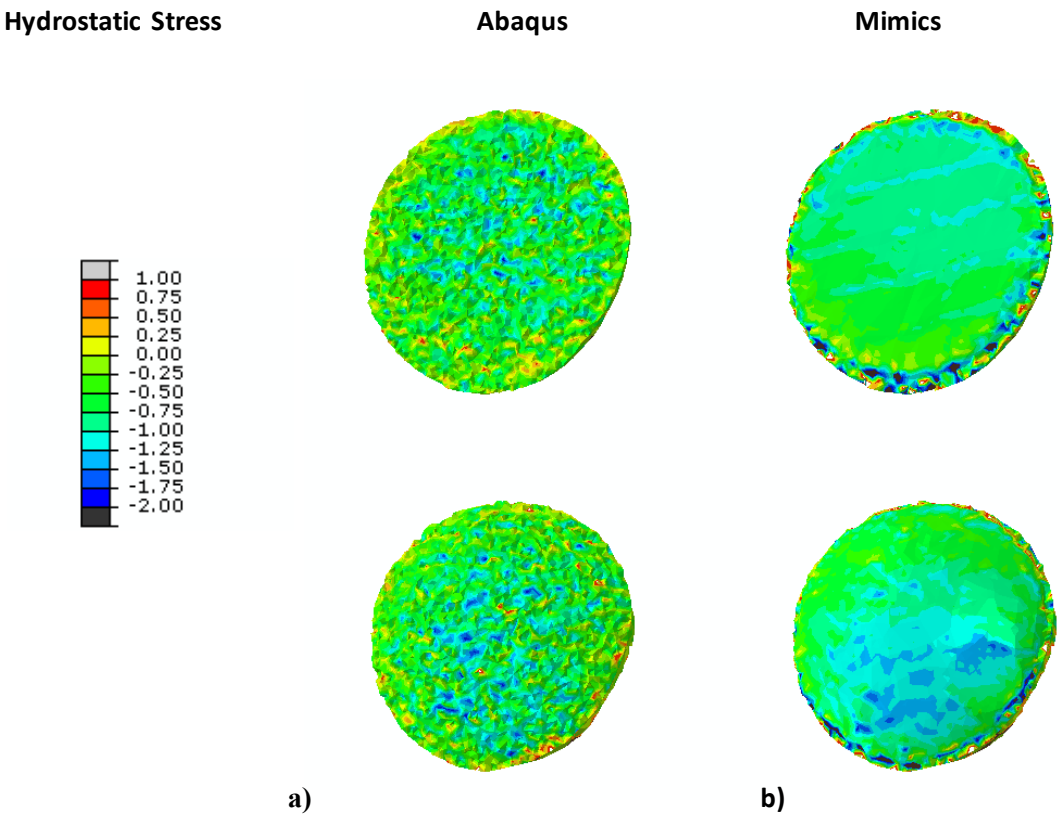

Fig. 9 *Hydrostatic Stress plots of the flat and convex growth plate corresponding to Fig. 8. Segmented in Abaqus (a) and Mimic (b).*

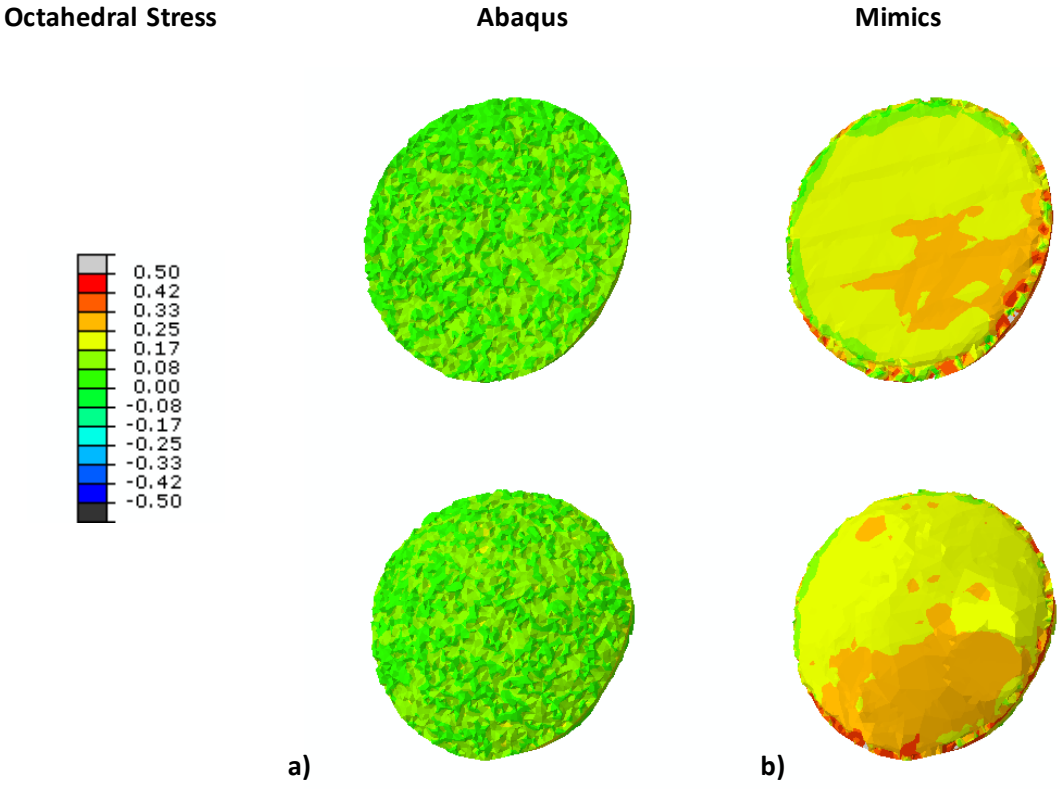

Fig. 10 *Octahedral shear Stress plots of the flat and convex growth plate corresponding to Fig. 8. Segmented in Abaqus (a) and Mimic (b).*

Flat vs. Convex Shape

In Fig. 11a, no growth plate is modeled, representing the situation where the growth plate is closed. The compressive and shear stress is gradually transmitted to the dense cortex of the diaphysis. Implementation of a flat growth plate alters the distribution in the proximal femur, by retaining part of the stress in the epiphysis. A convex growth plate shape strengthens this effect and the shear stress is distributed towards the sides. A tensile stress peak appears on top of the growth plate, while the growth plate and the region underneath the growth plate remain under compression. Overall, modeling of a growth plate causes higher stresses and strains in the epiphysis, and therefore a higher osteogenic index.

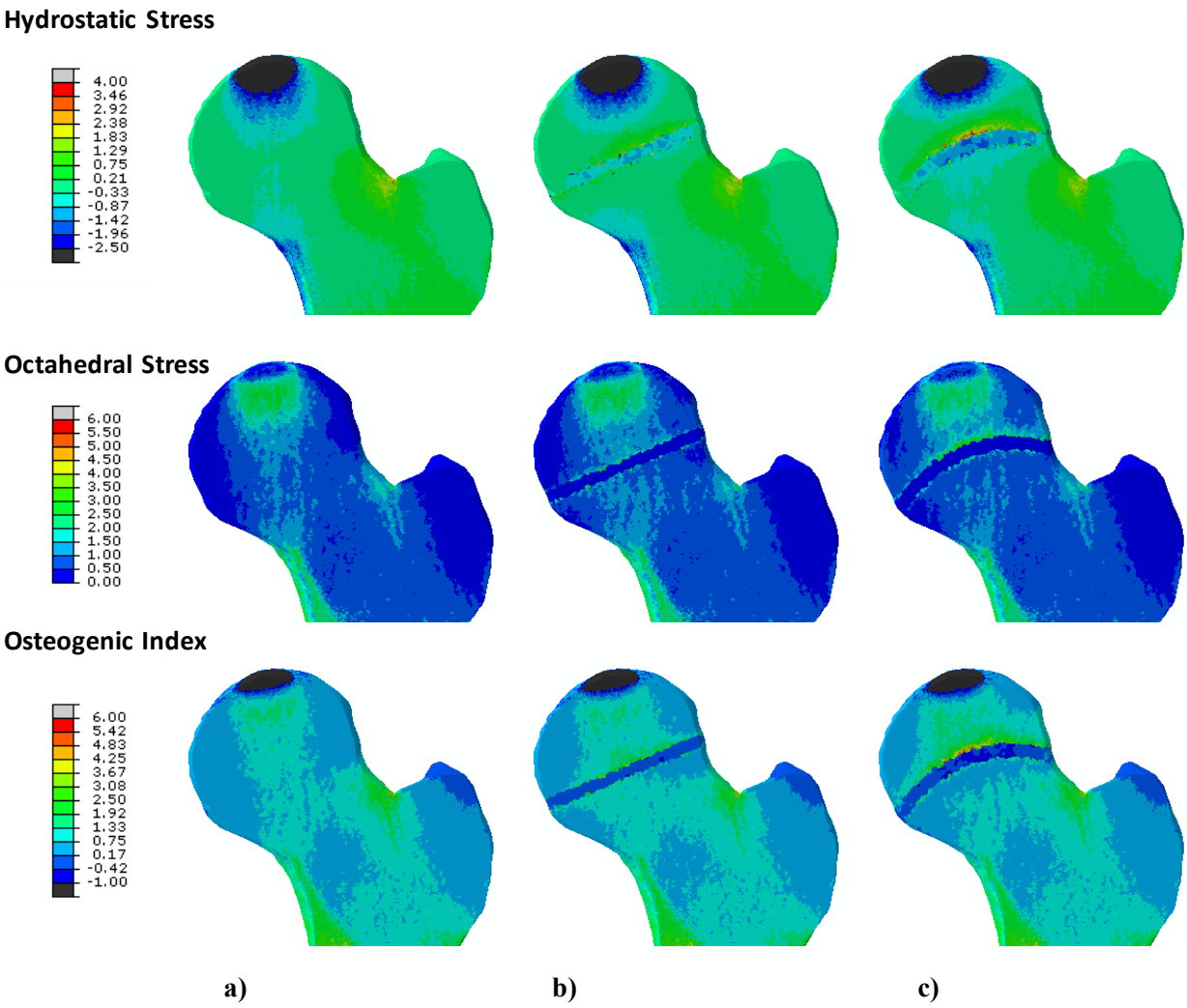

Fig. 11 *Stress distributions and osteogenic index distribution in cross-sections 6mm anteriorly from the femoral head center, at the location where a Cam might develop. All plots represent loading case 1 (a) without modeling of the growth plate, (b) with GP2 flat and (c) GP2 convex. The growth plate segmentation is completed in Abaqus.*

The hydrostatic stress and strain seem to be more homogeneously distributed in the flat growth plates. In the convex growth plates there appears a clear hydrostatic stress peak at the location closest to the impact force, which is then further distributed over the rest of the growth plate, Fig 9 and 12a. Tension and shear stresses at the medial side of the convex growth plate under loading Case 3 lead to an OI peak at the medial side, as depicted in Fig 13a. An extra model with a flat growth plat located higher in the femoral head depicted in Appendix 13, gave the same distinct pattern as the convex shape when the legend scale was adjusted. In order to further investigate the differences between a flat and convex shape an exploratory thick growth plate was modeled, Fig. 12b and 13b. A thicker growth plate shifts the compression region medially, this is especially true for the flat growth plate (Fig 12b), resulting in high growth index at the lateral side.

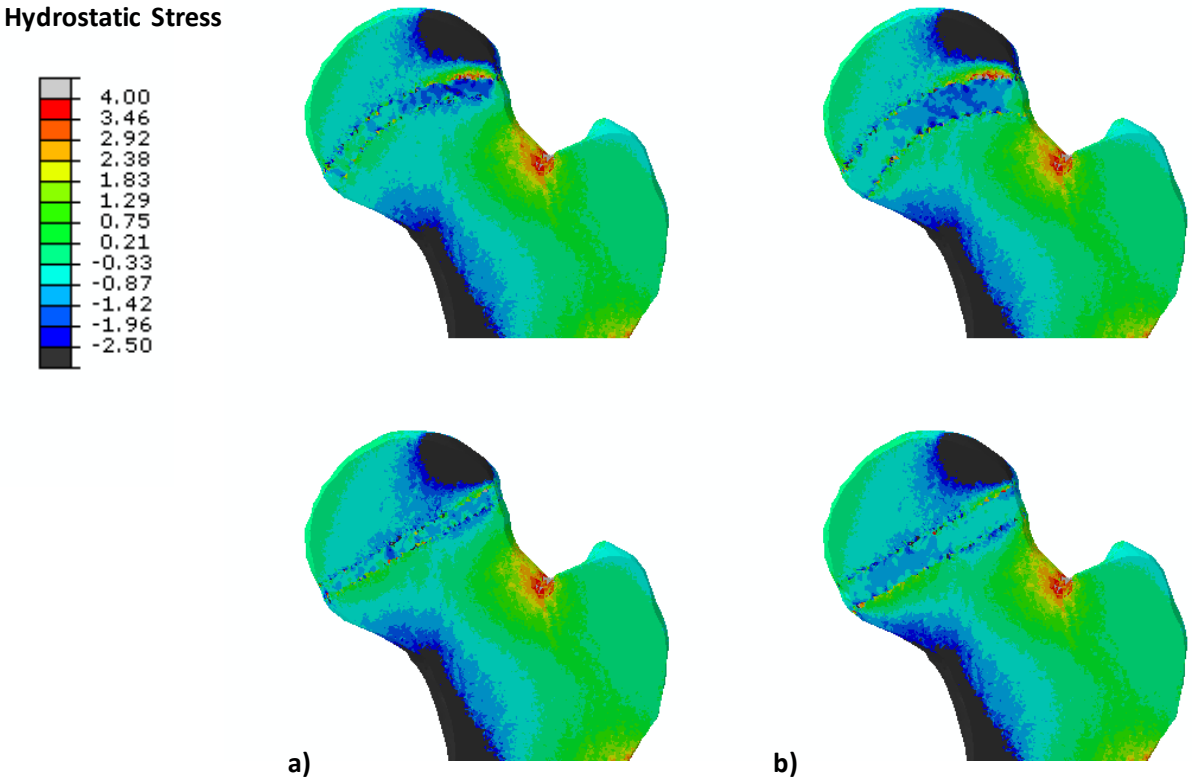

Fig. 12 *Hydrostatic stress contour plots under loading Case 3 with growth plate1convex(above) and flat (below) (a) 3mm and (b) 6mm.*

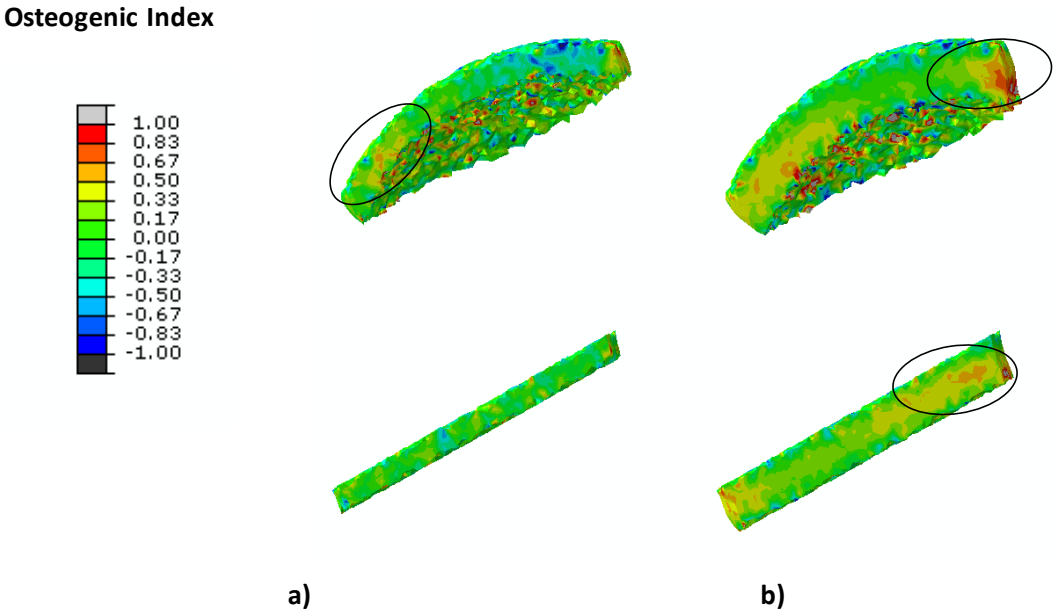

Fig. 13 *Osteogenic Index distribution of GP1convex(above) and flat (below) (a) 3mm and (b) 6mm.*

Loading Direction

In App 14-16, the osteogenic index distribution of the proximal femur of all loading scenarios and growth plate orientation is presented. A clear elevation in OI can be observed, when comparing the loading conditions C3 and C4 with C1 and C2. In case 3 the force induces a tensile peak in the neck. The difference in stress distribution due to the spatial configuration of the growth plate, is directly related to the direction of the hip contact force. When the impact force direction is perpendicular to the orientation of the growth plate, a compression peak inside the growth plate is in compliance with the location of the external force, which is higher and more concentrated the closer the impact force is situated to the surface of the growth plate, Fig. 14. If the force is more parallel oriented, the compression is distributed over the growth plate, for example in GP1 under Case3.

The osteogenic index contour plots of GP1 and GP3 under four loading conditions are presented in Fig.15. For GP1, loading Case 3 results in a compression peak at the lateral-anterior region, which is reflected by the low OI values in that same region. In loading case 2 the peak is located at the medial-anterior region. Higher growth rates appears when the load is directed more parallel to the growth plate axis on the opposite site of the contact force, as in the extreme loading scenario's 3 an 4. In GP3 under Case 3, the lateral edge occurs under tension resulting in high OI values laterally.

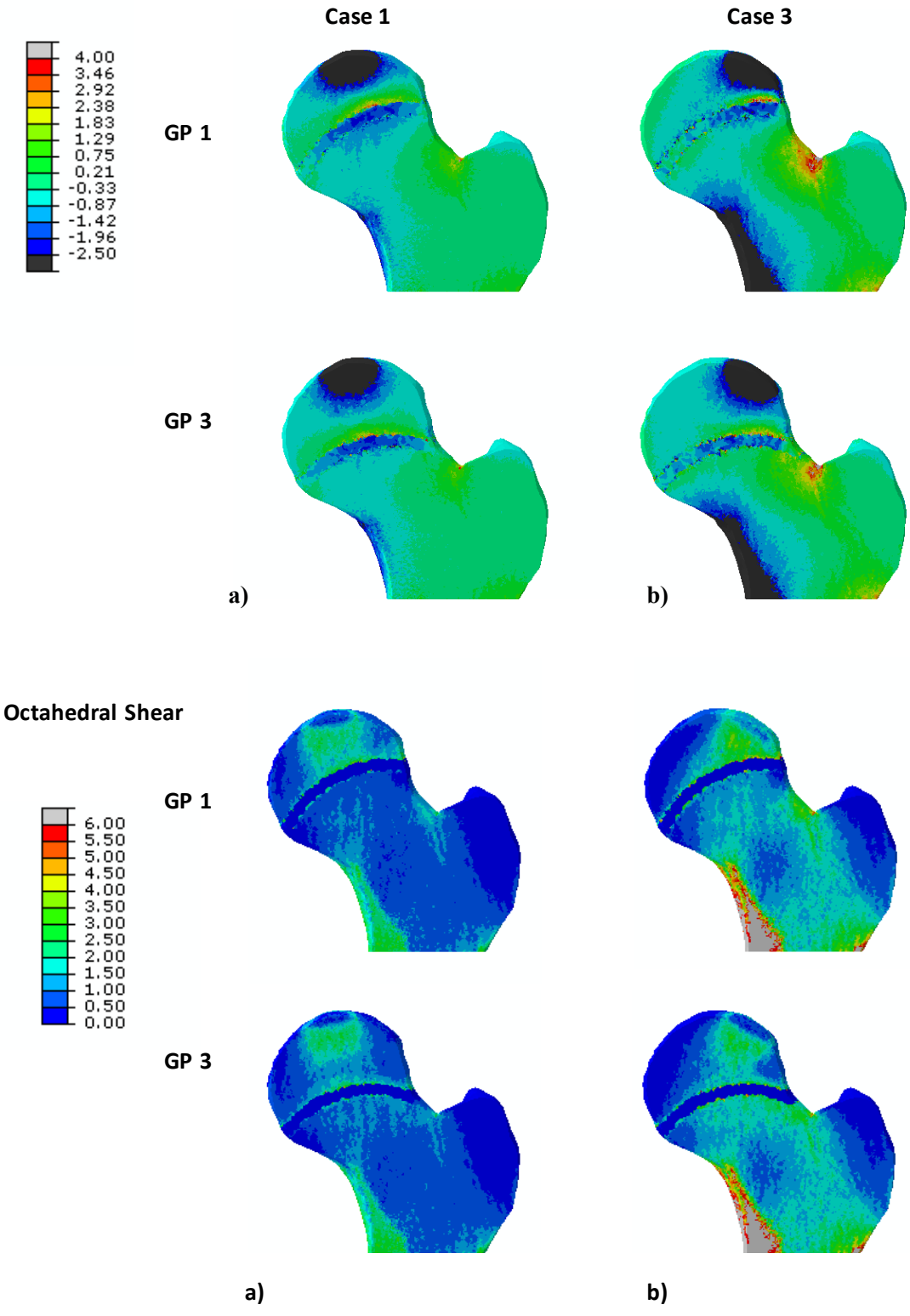

Fig. 14 *Hydrostatic and octahedral shear stress plots for of the femur with GP1 and GP3 under loading (a) Case 1 and (b) Case 3.*

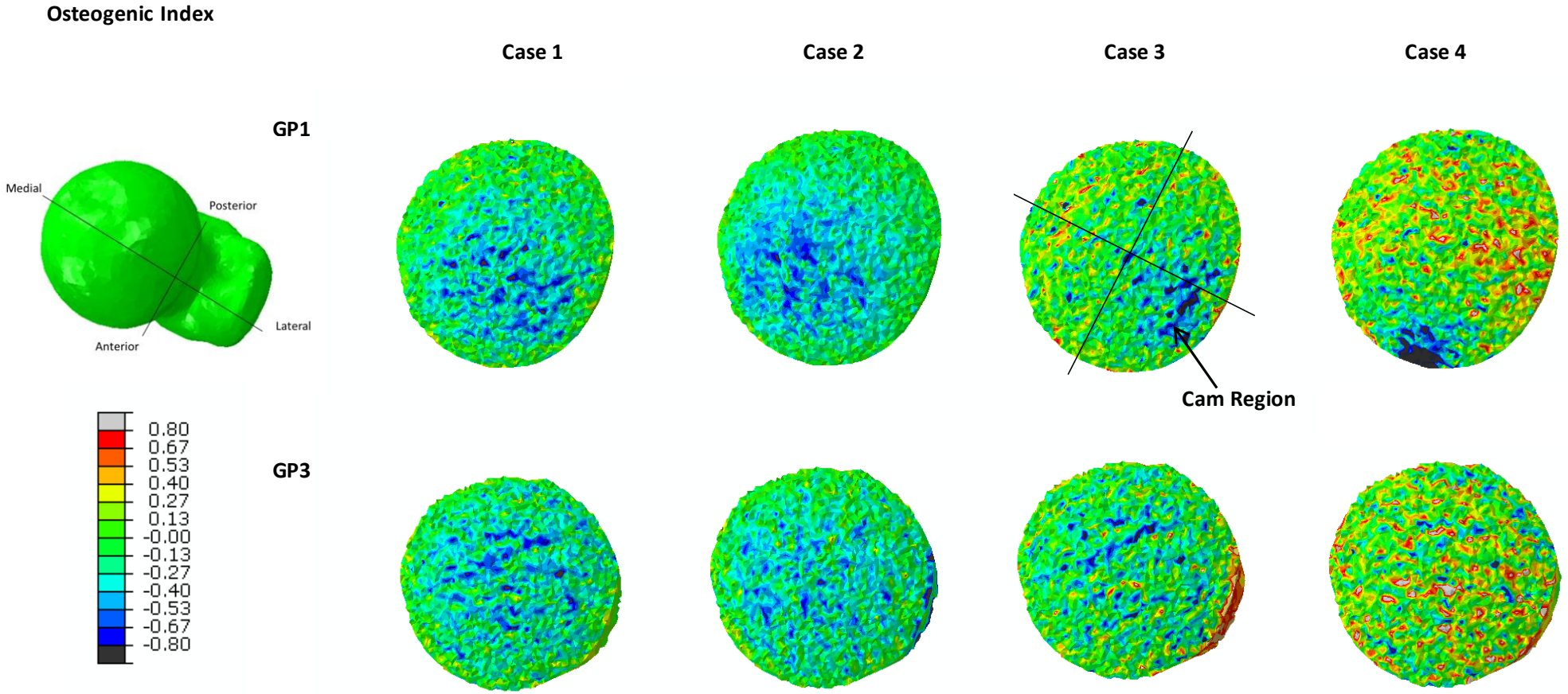

Fig. 15 *GP1 and GP3 under four loading conditions.*

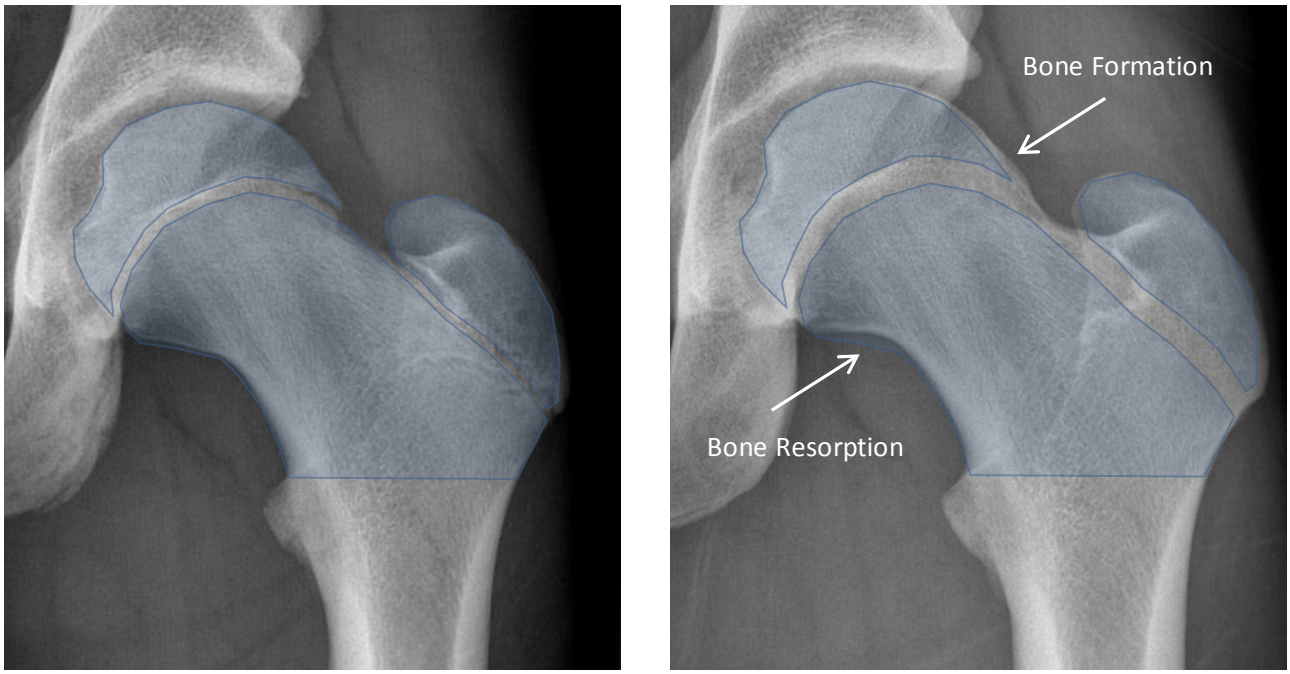

a)

b)

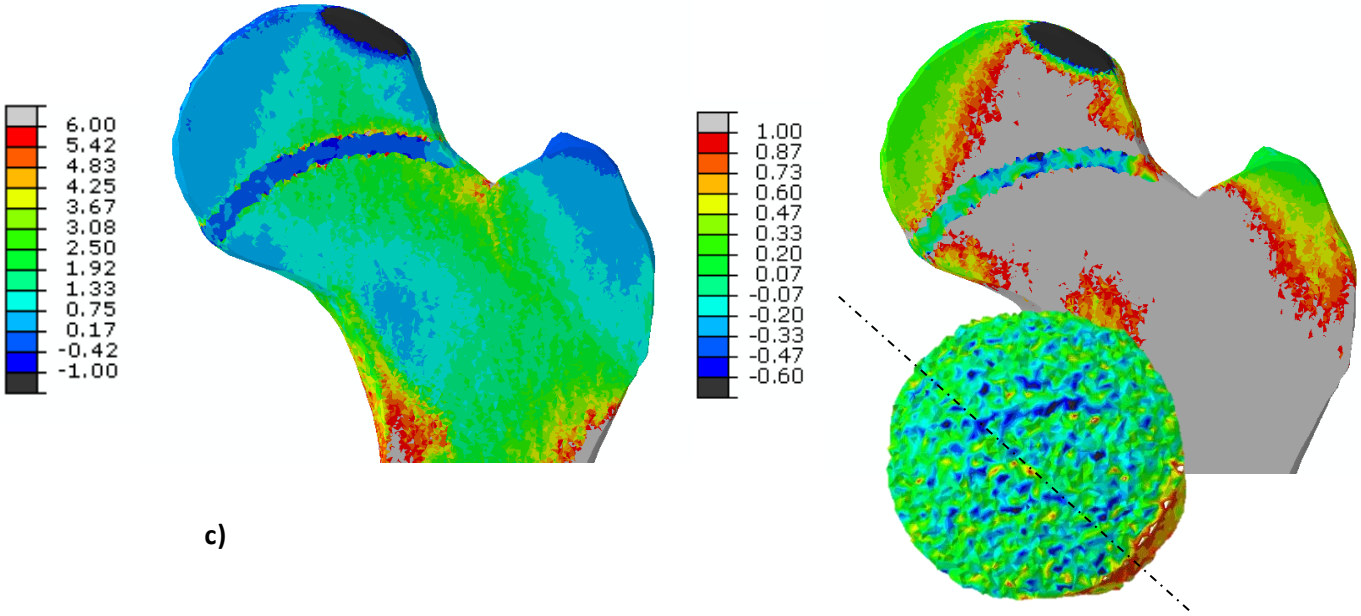

c)

Fig.16 *(a) Radiograph of a femur with an epiphyseal extension of Q1>1.6 at baseline and (b) Same femur at 2 year follow-up with alpha angle>60°. The blue contour indicates the shape and illustrate the growth region. (c) The Osteogenic Index distribution in the proximal femur for GP3 under loading Case 3. (Right) OI contour plot of the proximal femur and growth plate (Scaled).*

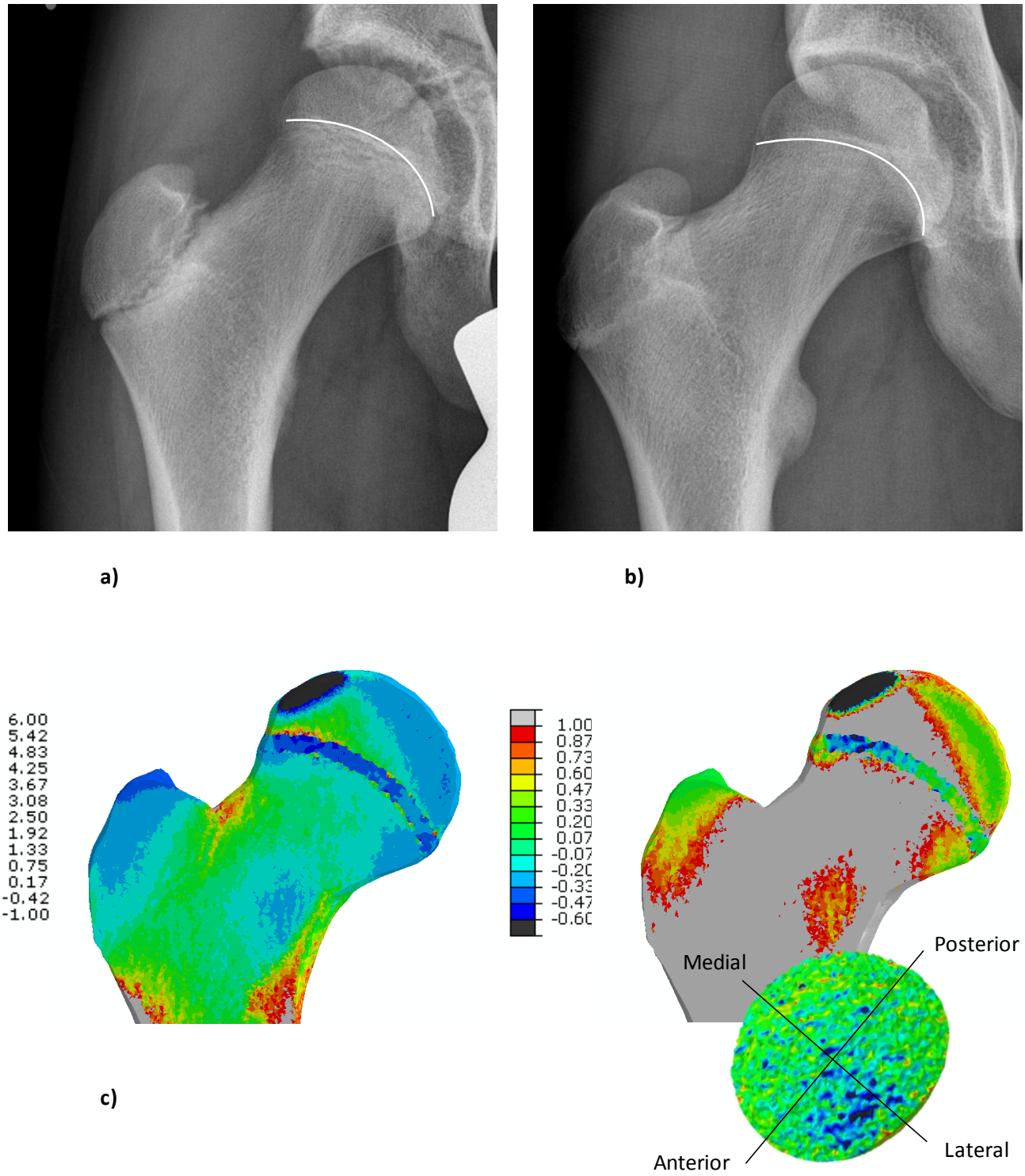

Fig. 17 *(a) Radiograph of a femur with an epiphyseal extension of Q1>1.4 at baseline and (b) 2 year follow-up.(c) The Osteogenic Index distribution in the proximal femur for GP2 under loading Case 3 (Right) Scaling indicates a region of low OI which could cause a deflection of the growth plate.*

A femur with an epiphyseal extension (Q1) of 1.6 at baseline and an alpha angle larger than 60° showed a prominence at two year follow-up, Fig 16 and App. 17. Bone resorption occurred inferior and bone formation anterosuperiorly. This hold for femurs that have an open growth plate at baseline. As depicted in Fig. 18, after epiphyseal closure the morphology does not change substantially. The osteogenic distribution plots of the proximal femur with GP3, which corresponds to Q1=1.6, under loading Case 3 shows high OI values in the epiphysis, distributed along the top of the growth plate towards the lateral side. Low OI values are found in the area under the medial side of the growth plate. The scaled plot and contour plot of the growth plate indicate high growth rates at the lateral edge of the growth plate. In figure 17, a hip with a low extension at baseline (Q1=1.2), deflect minimally at the anterosuperior side. Under the superior side of the growth plate low OI values are found. The high values are distributed along the growth plate.

a) **b)**

Fig. 18 *Radiographs of a femur (a) at baseline and (b) 2 year follow-up.*

Muscle Force & Trochanteric Growth Plate

Adding a tensile force on the greater trochanter does not directly influence the magnitude or distribution of the stress and strain in the epiphyseal growth plate or proximal femur, Fig. 19. In Case 3, it results solely in a local tensile and shear peaks at the surface of the greater trochanter, causing superficial high OI values. The effect of the muscle is more prominent when implementing a trochanteric growth plate. The plate distributes the shear and hydrostatic stress along its side, resulting in high OI peaks and low OI values inside the greater trochanter.

Case 2 - Muscle Force - Trochanteric GP

Hydrostatic Stress

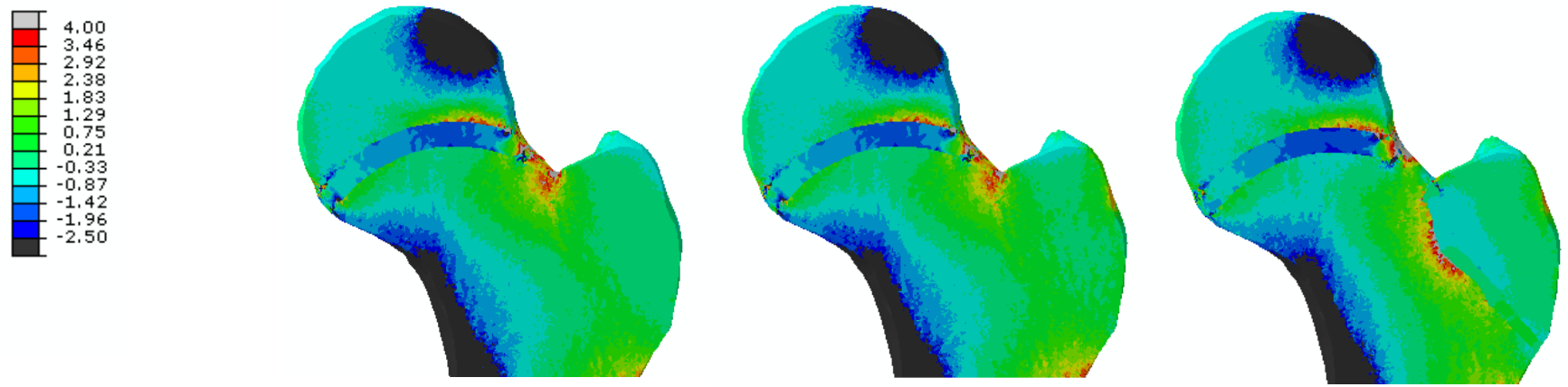

Osteoenic Index

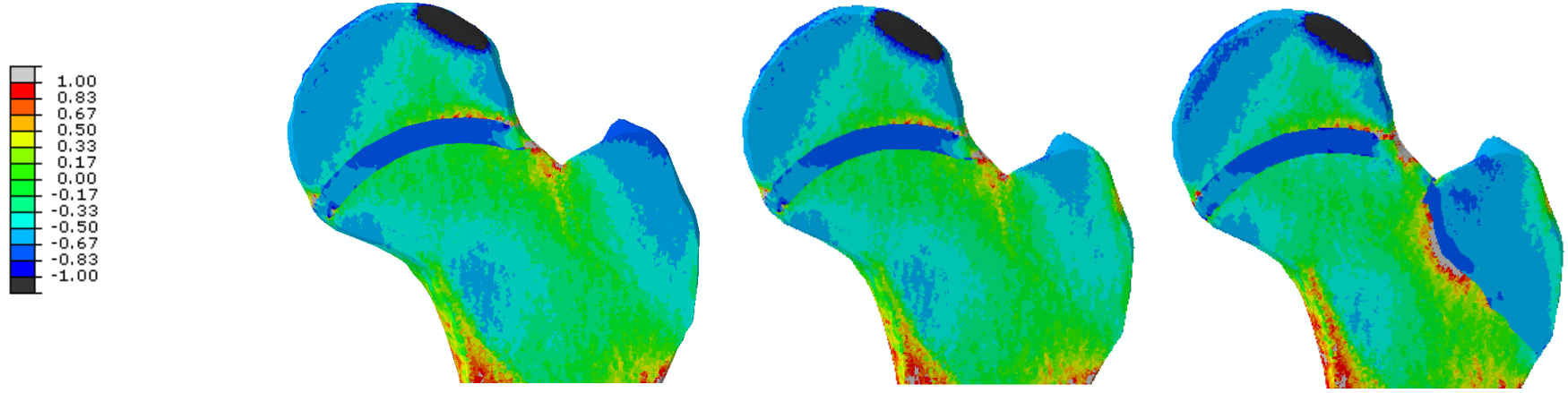

a) **b)** **c)**

Fig. 19 *Hydrostatic stress and osteogenic index distribution in for loading case 3. (a) GP3 (b) GP3 with muscle force(c) GP3 with trochanteric growth plate.*

4. DISCUSSION

4.1 Medical Image Analysis

The main goal of this research was to understand the development of a Cam-type deformity. The results from the image analysis confirm a positive correlation between the epiphyseal extension (Q1) and the alpha angle. This is in agreement with previous published data by Siebenrock et al. (30, 31). Furthermore, significant higher Q1 values are found in the Cam group for both open and closed growth plates. The statistical difference decreased after epiphyseal closure. Siebenrock et al. (30) conducted an epiphyseal extension analysis on 6 radial-sequence cut views for basketball athletes compared with an age related control group and found corresponding results. The athletes had a higher extension in all directions for open and closed physis, plus the difference with the control group decreased after closure of the growth plate.

The fact that the Q1 value was not a predicting factor in the development of a Cam-type deformity, might be because the measurements were carried out in a single AP pelvic plane. Considering the athletes group in the study of Siebenrock et al. (30), the epiphyseal extension increases after epiphyseal closure for the 2 and 3 o'clock position, corresponding to the results in this study on the AP pelvic view. However, for the 11 and 12 o'clock position the epiphyseal extension decreased, which was not seen in the control group. Kienle et al (75) states that there is almost no change in extension after the physis is closed, suggesting that this change occurs right before complete closure. These results were not found in this study, as the extension was not measured in those planes. Therefore, the development of a Cam might not be solely attributed to a higher epiphyseal extension at the anterosuperior region. The fact that after epiphyseal closure the posterior extension is lower, could be an important factor as well.

4.2 Abaqus vs. Mimics Segmentation

The segmentation protocol of the growth plate in Abaqus is much more convenient. In Mimics, multiple mesh generations are required followed by applying material properties and loads and

boundary conditions, while in Abaqus, only the section assignment of the growth plate material is adjusted. Mimics however, provides a more distinct pattern in the growth plate, since the stress and strain distribution is smoother. This is off course due to the fact that the surface of the growth plate is taken into account when generating the mesh. This is in agreement with both Carriero (73) and Fishkin (54), who also include the growth plate in the mesh generation. The surface of the edge of the growth plate made in Mimics is rough, as those elements were added after the mesh generation in Abaqus. This results in the high and low stress peaks that are seen on the edge of the growth plate, which in reality are not there. This problem can easily be resolved by using local Boolean tool in 3-Matic, and selecting the surface of the growth plate as elite 1 and the inner surface of the femur as elite2. Unfortunately, for this research this toolbox was not available. The octahedral shear stress, and consequently the osteogenic index, is lower when the GP is segmented in Abaqus. This also applies to the octahedral shear strain. The lower shear values can be attributed to geometrical resistance. Although the contour plots of the growth plate segmented in Mimics provides more clear information, it cannot be concluded that they are more realistic. The local stress and strain peaks inside the growth cartilage as well as in the adjacent trabecular bone that are seen in the Abaqus segmentation, may occur when the growth plate has a dimpled surface. When analyzing the CT images, the epiphyseal plate is also not defined by a perfect sphere. It has an irregular and convoluted surface (76), which increases the contact area between the epiphysis and metaphysis providing stability (77), causing resistance to the strain in some extent.

4.3 Stress Distribution Growth Plate

The flat growth plate shows a homogeneous hydrostatic stress distribution, while in the models of Fishkin et al. (54) and Carriero et al.(73) a distinct pattern appears. This difference could be explained by the position of the growth plate rather than the shape. The distance from the proximal surface of the model where the force is applied is larger for the flat growth plate than for the convex one. The concentration is blurred, which is also described by the concave model of Piszczatowski et al.(78).

For Carriero, who placed the growth plate even lower in the neck region, the distinct hydrostatic stress distribution could be explained by the fact that the geometry of the femoral head and neck alters

the stress distribution before it researches the growth plate. When analyzing the stress distribution in the femur without growth plate in for instance Case 1 App. 14, a tensile peak can be seen in the superior portion of the neck. This corresponds to the results by Carriero, who found tensile stress on the lateral portion of the growth plate for 'normal' load (Case 1). Shefelbine (74) also found hydrostatic tension and higher octahedral shear stresses on the lateral part of the growth region, leading to a higher growth rate on the lateral side for normal loading. Under CP loading no hydrostatic tension appears, causing less growth at the medial side. Both studies do not shows the distribution in the femur, however as stated before, the geometry of the femoral head and neck and the position of the growth plate determine might influence the stress distribution inside the growth plate. For both cases, the shear stress contributes to the OI distribution. As the growth plate in this study is positioned high in the femoral head, representing the morphology of a 12 year old, the hydrostatic pressure is not passed to the lateral side via the neck, but is retained by the growth plate at the location of the force. Resulting in a high compression peak in the growth cartilage that appear at the location of impact result in less growth. Furthermore, a relatively homogeneous octahedral shear stress distribution resulting from a force perpendicular to the growth front appears. That is why the shear stresses does not influence the OI distribution only the magnitude. Consequently, the growth rate is directly related to the location of the contact force. This is in line with the results of Piszczatowski et al. (78), who stated that the region of lower mechanical stimuli follows the direction of the maximum force and the maximum OI appears in the parts where the cartilage surface is almost parallel to the loading direction. In the loading case 3 and 4, which represent the extreme range of motions, the forces are more aligned with the growth plate axis. Indeed higher shear stresses are observed and bone growth is promoted at the opposite side from where the force is applied, Figure 13. Piszczatowski did found high OI values for loading under 45º (L4) and asymmetrical loading (L5) in the bottom right corner, this effect is stronger in a thicker growth plate. Furthermore, a thicker growth plate could lead to a shift in the compression region. These results correspond to the findings in this paper. Additionally, Piszczatowski concluded a more distinctive minimum is presented for the thin growth plates. Varying the thickness along the growth plate could lead to better understanding if a more medial directed force could lead to higher osteogenic activity in the Cam region. Furthermore, the closer the external force is

to the growth plate, the more distinct and higher the compression stress region is. Since athletes might be subjected to forces in a more extreme range of motion, it could be assumed that they experience higher compression and shear stresses in the growth plates. Which could lead to the irregular and partly opened growth plates which are seen in athletes (79). The actual shape of the growth plate changes considerably over time. For this model, a convex shape higher in the head appears more realistic. At the age of 13, the flat convoluted surface develops into a mild arc that is regular and smooth (77), which is also observed when analyzing the X-rays. However, as is stated earlier in the discussion, less extension of the growth plate after epiphyseal closure can be observed locally at the posterior-superior region in athletes. Therefore, it can be concluded that both flat and convex shapes are not able to incorporate all the physiological aspects. Furthermore, the thickness and the exact location of the growth plate should be considered as the geometry of the femoral head and neck seems to alters the stress distribution before it researches the growth plate.

4.4 Stress Distribution Femur

Both Carriero and Fishkin do not discuss the stress distribution in the surrounding proximal femur. Due to the lack of experimental results and comparable studies, the cross-sectional contour plots of the femur can give only an indication on the stress distribution when modeling a growth plate. The high regional stresses and osteogenic index that appear in the epiphysis when modeling a growth plate could stimulate local bone remodeling and apposition. This especially applies to the convex growth plate with perpendicular loading, where a tensile peak appears on top of the growth plate at the location of the force and the shear stress is distributed towards the sides. If the force is positioned at the anterosuperior surface, as in Case 3, local high stresses in epiphysis encourages bone remodelling and could lead to overgrowth of bone into the femoral neck. After epiphyseal closure, presented by the models without growth plate, the stress is no longer retained in the epiphysis but transmitted towards the shaft. Indicating that a child's femur is more affected by the hip contact forces than a mature skeleton. If you analyze the hydrostatic stress distribution in the femur for all loads, the hydrostatic pressure was the greatest directly under the applied load. If the contact force is vertical the stress is guided towards the medial shaft (Case 1 and 3). When the load is applied under a greater angle, more

lateral, the compression stress transfers via the neck region towards the lateral part of the shaft (Case 2) and hydrostatic tension occurs in the medial portion. Same results are found in the research of Shefelbine (65). Their model is based on a neonatal geometry; the head and neck are not formed yet and the growth front is placed in the diaphysis. Therefore, the more lateral positioned force seen in patients with developmental dysplasia of the hip (DDH) result in hydrostatic tension and consequently bone growth at the medial side.

The studies of Carter, Shefelbine and Carriero analyze the general growth direction by predicting the anteversion angle and neck shaft angle. No previous study investigates local excessive growth, like the Cam-bump. The growth plate orientation changes such that it is perpendicular to the loading direction. Regions that are subjected to shear will grow, allowing to obtain complete compression, Fig 20a. In Case 3 the force results in high compression forces inside the growth plate in the anterosuperior region, leading to less endochondral bone growth in the Cam region. The resulting deflection of the epiphyseal plate, might be visible in Cam patients as higher extension. Higher OI values in the deflected area as seen in the study of Piszczatowski, could lead to endochondral growth into the neck (Fig 20c). Otherwise, the accompanied local higher stresses in the epiphysis could stimulate local bone remodeling and apposition in the anterosuperior region. This effect could be stimulated by the shear stresses that might occur due to the lower extension of the plate posteriorly, as was measured by Siebenrock et al. (80). These results would support the theory that a Cam-type deformity might not be a result of endochondral growth, but the morphological changes during ossification alter the local remodeling and apposition, Fig. 20d.

The load direction has a great influence on the mechanical stimuli within the growth plate as well as in the femur. A limitation of this research are the hypothetical loading conditions. Accurate quantification of internal hip forces remains difficult for both practical and ethical reasons. ‘Smart’ implants with implemented measurement instruments can be used to measure the force directly inside a patient. Bergmann et al. (47) provided direct in situ dynamic force and motion measurements based on instrumented implants during a variety of daily activities. Unfortunately, there is limited knowledge on hip loading conditions that correspond to high impact sports. Using musculoskeletal models, the joint reaction and muscle forces under specific movements can be estimated in the absence of

experimental data. Those models use inverse dynamics to calculate the internal moments and forces, based on the ground reaction force and kinematic data. Since conducting a kinematic analysis is beyond the scope of this research, quasi-static loading conditions are assumed based on existing literature. The implementation of the muscle force should provide a more realistic model. As they play an important role in the development of the lateral part of the femur. However, in this model the tensile force does not directly influence the magnitude or distribution of the stress and strain in the epiphyseal growth plate or epiphysis. Modeling of the trochanteric growth plate gradually guides tensile peak in the neck observed Case 3 towards the lateral shaft.

4.5 Growth Analysis

Although the Carter's mechanobiological is sensitive to the interrelation between growth plate orientation and force direction, it seems that the hydrostatic stress direction almost completely determines the region of reduced mechanical stimuli. In this study a b/a ratio of 0.5 was used, in order to analyze the bone growth. The ration a/b must be between 0.3 and 1, to simulate a proper endochondral ossification process (81). When using a higher ratio, the hydrostatic stress will become more significant, and the results will resemble Stokes axial approach (78). A decrease in ratio will increase the influence of shear, and thus the sensitivity to the shape of the growth plate. Ribble et al. (82) used just shear stresses to predict the development of the neck shaft angle. It has been suggested that in later development, the importance of the compressive stress decreases in the lateral metaphysis, while the shear stress in the plane of the epiphyseal plate will increase (83), suggesting that the ratio should be adapted according to age. Overall, these finding al indicate the need for further research into the shear and compressive stress ratio.

In addition, Several studies indicate that static compression of cartilage decreases biosynthesis, while cyclic compression increases biosynthesis (84, 85). Carter's model does not allow to simulate bone growth in a compressed part of the physis.

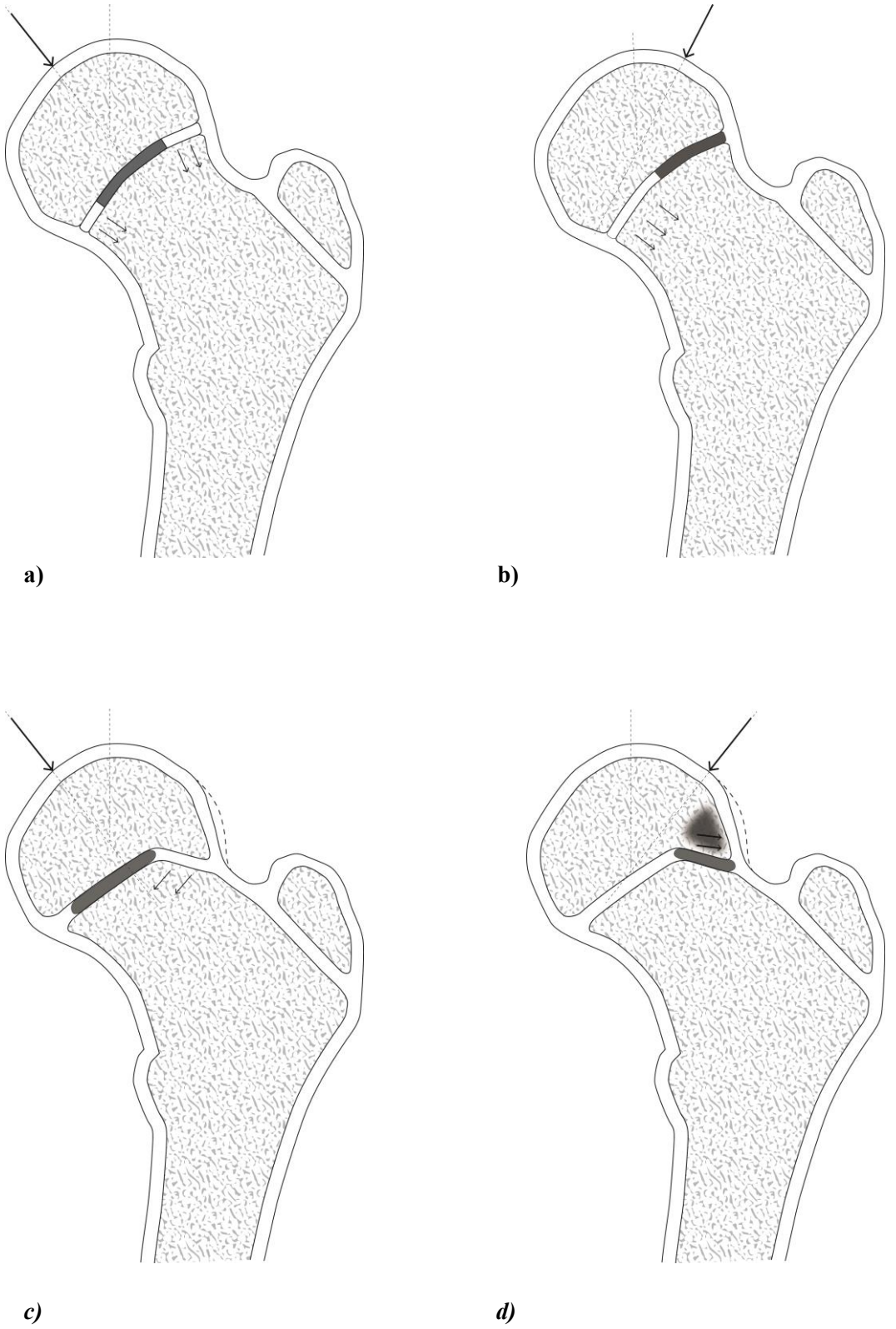

Fig. 20 *Development of the hip during childhood occurs by proliferation at the growth cartilage (white areas). (a) Load directed perpendicular to the growth plate, (b) A more medial directed load causing a lateral compression region, resulting in a deflection of the growth plate into the femoral neck visualized in c and d, (c)Under normal loading, the defected area experiences shear stress, which might stimulate growth in the lateral direction. (d) High stress zones in the superior anterior region of the epiphysis could result in bone apposition and extension towards the neck.*

4.6 Stress and Strain Magnitudes

Although, the focus of this research was on stress distribution the overall stress magnitudes in the growth plate are acceptable. The shear stress values of 0.5MPa are in line with previous studies of Carriero (73) and Shefelbine (74), who both studied morphological changes of children with cerebral palsy (CP). These values are well below the threshold value of 1.164MPa for shear failure load in a cadaveric 13 year old female reported by Chung et al. (86). Williams et al. (87) stated the magnitudes of 0.98±0.9MPa for ultimate stress and 31%±7% for ultimate strain. The 15% shear strain that is observed in the growth plate fall below this values. The more parallel the growth plate is with the direction of force, the higher the shear stresses. When comparing the shear stress in GP1 under loading case 2 and 3, a difference of 0.25MPa in can be observed (App. 20). Which corresponds to the literature. Zupanc et al. (88) used a mathematical model to calculate shear stresses in the growth plate and found values of 0.81Mpa for the vertical growth plates (55.4º) and 0.51MPa (63.2º). Higher hydrostatic stresses of 2MPa were found, compared with Carriero and Shefelbine, the positioning of the growth plate could be an explanation for this, as it is much closer to the force impact region, especially for the loading cases 3 and 4, which are not evaluated in the other studies. The hydrostatic strain of course almost zero, as the growth plate is modeled as incompressible material.

4.7 Recommendations for future research

In the future, a more realistic orientation and shape of the growth plate can be realized by using a spine function to describe the upper and lower line of the growth plate. Local deflections and difference in thickness will be taken into account that influence the stress distribution in and around the growth plate. The spine function can be based on the same 22 landmarks that annotate the upper and lower boundary of the growth in the medical image analysis. Currently, the orientation of the growth plate in the 3D model is based on measurements done on 2D images in the AP pelvic view. The landmarks of the lateral view can be used generate a complex shape in 3D, including the change in extension posteriorly. Unfortunately, visual landmark based registration is challenging and time consuming. The edge of the growth plate, especially the lower boundary, is very unclear on CT scans. Interesting

would be to do the same measurements on the follow-up scans, to measure the exact change in deflection of the growth plate towards the lateral side.

The spine function can be implemented in Abaqus or Mimics on multiple femoral geometries. As the segmentation process is very time consuming, the geometry of this model is based on only one femur. Which is more realistic than other studies that use parameterized/idealized ball and socket model or CAD model from previous articles. Yet, the femoral shaft is short to reduce the amount of radiation when making the scans. Therefore, the distal fixation ensures forces that account for the actions of muscle forces might influence the local stress and strain distribution in the femoral neck and physis.

When the geometry is parameterize, the influence of a reduced femoral neck-shaft angle, which was observed in the Cam group, could be investigated. In subject specific modeling, the growth plate can directly be segmented in Mimics to obtain the actual 3D shape, thickness and orientation. For this, MRI images would be the best solution as the shape of the growth plate is best visualized on MRI (77).

They accuracy of the loading conditions is have a great influence on the stresses within the growth plate, this study limited by assumption of static analysis. An extensive motion analysis of a child, would be the optimal solution in order to calculate the hip contact forces and muscle force acting on the juvenile hip joint, during specific soccer/basketball related movements. The lower limb model of the OpenSim musculoskeletal database can be used for this purpose (89). The dynamic loading conditions, include the direction and magnitude of the force over time, could be imported into Abaqus.

The mechanical behavior is strongly dependent on the material assignment (90). Therefore, a more realistic material would be of added value. Although the strain do not exceed the ultimate values, Neo-Hookean, hyperelastic material model can be used to predict the highly nonlinear behavior of the physis. Beside, when implementing dynamic loading, the viscoelastic properties of the growth plate are interesting to analyze.

A further step would be to simulation bone growth and ossification, by implement the mechanobiological principles in iterative FE model. A disadvantage of the Carter's model is that it does include the direction of growth. Carriero and Shefelbine use the average deformation of the growth plate to calculate growth direction. When implementing tissue growth and adaptation, the

stress distribution changes over time due to the change in geometry of the femur. Additionally, include the bone remodeling process and explore the possibilities to simulate local bone apposition. This allow for a much more realistic growth prediction. Beside mechanical stimuli, biological factors influence the growth rate as well. Especially, close to skeletal maturity, when the mechanical factor have a smaller influence on bone shape (74). When there is no mechanical loading on bone, it still grows 50 to 80% of its normal size. The biological component includes hormonal and genetic regulation and can be calculated by;

$$\dot{\varepsilon}_b = \frac{\dot{r}}{l_0} \tag{7}$$

where, $\dot{r}$ is the experimentally determined growth rate (mm/day) and l_0 is the length of the growth region (mm). This factor is not included in this research, but should be interesting to take into account as practicing sports might influences the growth hormone regulation (91).

To conclude, this research is only the first step in understanding the development of a Cam deformity. The current level of knowledge allows us to analyze the stress distributions inside de femur and growth plate when implementing a growth front, however it remains a rough approximation of the in vivo situation. It will be an ongoing challenge to understand how physical activity during skeletal development will influence the femoral morphology.

REFERENCES

1. Fish JR, Beall DP, Sweet CF, Martin HD, Lastine CL, Grayson DE, et al. Imaging findings of femoroacetabular impingement syndrome. Skeletal Radiol. 2005;34(11):691-701.
2. Leunig M, Ganz R, Leunig-Ganz K, Harris WH. The etiology of osteoarthritis of the hip - An integrated mechanical concept. Clinical orthopaedics and related research. 2008;466(2):264-72.
3. Ganz R, Parvizi J, Beck M, Leunig M, Notzli H, Siebenrock KA. Femoroacetabular impingement: a cause for osteoarthritis of the hip. Clin Orthop Relat Res. 2003(417):112-20. Epub 2003/12/04.
4. Lavigne M, Parvizi J, Beck M, Siebenrock KA, Ganz R, Leunig M. Anterior femoroacetabular impingement: part I. Techniques of joint preserving surgery. Clinical orthopaedics and related research. 2004;418:61.
5. Pfirrmann CW, Mengiardi B, Dora C, Kalberer F, Zanetti M, Hodler J. Cam and pincer femoroacetabular impingement: characteristic MR arthrographic findings in 50 patients. Radiology. 2006;240(3):778-85. Epub 2006/07/22.
6. Bardakos NV, Villar RN. Predictors of progression of osteoarthritis in femoroacetabular impingement A RADIOLOGICAL STUDY WITH A MINIMUM OF TEN YEARS FOLLOW-UP. J Bone Joint Surg Br. 2009;91B(2):162-9.
7. Meyer DC, Beck M, Ellis T, Ganz R, Leunig M. Comparison of six radiographic projections to assess femoral head/neck asphericity. Clinical orthopaedics and related research. 2006(445):181-5.
8. Notzli H, Wyss T, Stoecklin C, Schmid M, Treiber K, Hodler J. The contour of the femoral head-neck junction as a predictor for the risk of anterior impingement. J Bone Joint Surg Br. 2002;84(4):556.
9. Ito K, Minka-II MA, Leunig M, Werlen S, Ganz R. Femoroacetabular impingement and the cam-effect - A MRI-based quantitative anatomical study of the femoral head-neck offset. J Bone Joint Surg Br. 2001;83B(2):171-6.
10. Clohisy JC, Knaus ER, Hunt DM, Lesher JM, Harris-Hayes M, Prather H. Clinical presentation of patients with symptomatic anterior hip impingement. Clinical Orthopaedics and Related Research®. 2009;467(3):638-44.
11. Burnett RSJ, Rocca G, Prather H, Curry M, Maloney WJ, Clohisy JC. Clinical presentation of patients with tears of the acetabular labrum. JOURNAL OF BONE AND JOINT SURGERY-AMERICAN VOLUME-. 2006;88(7):1448.
12. Buck FM, Hodler J, Zanetti M, Dora C, Pfirrmann CWA. Ultrasound for the evaluation of femoroacetabular impingement of the cam type. Diagnostic performance of qualitative criteria and alpha angle measurements. European radiology. 2010:1-9.
13. Beck M, Leunig M, Parvizi J, Boutier V, Wyss D, Ganz R. Anterior femoroacetabular impingement: part II. Midterm results of surgical treatment. Clinical orthopaedics and related research. 2004;418:67.
14. Larson CM, Giveans MR. Arthroscopic Debridement Versus Refixation of the Acetabular Labrum Associated With Femoroacetabular Impingement. Arthroscopy-the Journal of Arthroscopic and Related Surgery. 2009;25(4):369-76.
15. Lincoln M, Johnston K, Muldoon M, Santore R. Combined arthroscopic and modified open approach for cam femoroacetabular impingement: a preliminary experience. Arthroscopy. 2009;25(4):392-9. Epub 2009/04/04.
16. Naal FD, Miozzari HH, Wyss TF, Notzli HP. Surgical Hip Dislocation for the Treatment of Femoroacetabular Impingement in High-Level Athletes. Am J Sport Med. 2011;39(3):544-50.
17. Agricola R, Bessems JHJM, Ginai AZ, Heijboer MP, van der Heijden RA, Verhaar JAN, et al. The Development of Cam-Type Deformity in Adolescent and Young Male Soccer Players. The American journal of sports medicine. 2012.

18. Leunig M, Casillas MM, Hamlet M, Hersche O, Nötzli H, Slongo T, et al. Slipped capital femoral epiphysis: early mechanical damage to the acetabular cartilage by a prominent femoral metaphysis. Acta Orthop. 2000;71(4):370-5.
19. Rab GT. The geometry of slipped capital femoral epiphysis: implications for movement, impingement, and corrective osteotomy. J Pediatr Orthop. 1999;19(4):419-24. Epub 1999/07/21.
20. Hosalkar HS, Pandya NK, Bomar JD, Wenger DR. Hip impingement in slipped capital femoral epiphysis: a changing perspective. Journal of Children's Orthopaedics. 2012:1-12.
21. Snow SW, Keret D, Scarangella S, Bowen JR. Anterior impingement of the femoral head: a late phenomenon of Legg-Calve-Perthes' disease. Journal of Pediatric Orthopaedics. 1993;13(3):286-9.
22. Juul A. The effects of oestrogens on linear bone growth. Apmis. 2001;109(S103):S124-S34.
23. Murray R. The aetiology of primary osteoarthritis of the hip. British Journal of Radiology. 1965;38(455):810.
24. Eijer H, Myers SR, Ganz R. Anterior femoroacetabular impingement after femoral neck fractures. Journal of orthopaedic trauma. 2001;15(7):475.
25. Strehl A, Ganz R. Anterior femoroacetabular impingement after healed femoral neck fractures. Unfallchirurg. 2005;108(4):263-+.
26. Siebenrock KA, Ferner F, Noble PC, Santore RF, Werlen S, Mamisch TC. The Cam-type Deformity of the Proximal Femur Arises in Childhood in Response to Vigorous Sporting Activity. Clin Orthop Relat Res. 2011. Epub 2011/07/16.
27. Fraitzl CR, Kappe T, Reichel H. Femoroacetabular Impingement - a Frequent Cause for Groin Pain in the Athlete. Deutsche Zeitschrift Fur Sportmedizin. 2010;61(12):292-8.
28. Batt ME, Keogh MJ. A Review of Femoroacetabular Impingement in Athletes. Sports Med. 2008;38(10):863-78.
29. Ng VY, Ellis TJ. More than just a bump: cam-type femoroacetabular impingement and the evolution of the femoral neck. Hip international : the journal of clinical and experimental research on hip pathology and therapy. 2011;21(1):1-8. Epub 2011/02/01.
30. Siebenrock KA, Behning A, Schwab JM. Growth plate alteration precedes cam-type deformity in elite basketball players. Clinical Orthopaedics and Related Research®. 2012:1-8.
31. Siebenrock K, Wahab KA, Werlen S, Kalhor M, Leunig M, Ganz R. Abnormal extension of the femoral head epiphysis as a cause of cam impingement. Clinical orthopaedics and related research. 2004;418:54-60.
32. Carter D, Van der Meulen M, Beaupre G. Mechanical factors in bone growth and development. Bone. 1996;18(1):S5-S10.
33. Timothy A. Mirtza c, Judy P. Chandlerb, Christina M. Eyersb. The Effects of Physical Activity on the Epiphyseal Growth
Plates: A Review of the Literature on Normal Physiology
and Clinical Implications. Journal compilation © J Clin Med Res and Elmer Press™. 2010;3(1):1-7.
34. Saxon L. Role of exercise in the development of bone strength during growth. Deakin University, 2012.
35. Rohlmann A, Mössner U, Bergmann G, Kölbel R. Finite-element-analysis and experimental investigation of stresses in a femur. Journal of biomedical engineering. 1982;4(3):241-6.
36. Huiskes R, Chao E. A survey of finite element analysis in orthopedic biomechanics: the first decade. J Biomech. 1983;16(6):385-409.
37. Chegini S, Beck M, Ferguson SJ. The effects of impingement and dysplasia on stress distributions in the hip joint during sitting and walking: a finite element analysis. Journal of Orthopaedic Research. 2009;27(2):195-201.
38. Ng KCG, Rouhi G, Lamontagne M, Beaulé PE. Finite Element Analysis Examining the Effects of Cam FAI on Hip Joint Mechanical Loading Using Subject-Specific Geometries During Standing and Maximum Squat. HSS Journal®.1-7.

39. Suppanee R, Wong P, Esat I, Chizari M, Rajakulendran K, Bardakos NV, et al. The Kinematics of the Hip Joint with Femoroacetabular Impingement May Be Affected by the Thickness of the Articular Cartilage. Biomedical Imaging and Computational Modeling in Biomechanics. 2012:39-54.
40. Alonso-Rasgado T, Jimenez-Cruz D, Bailey CG, Mandal P, Board T. Changes in the stress in the femoral head neck junction after osteochondroplasty for hip impingement: A finite element study. Journal of Orthopaedic Research. 2012.
41. Nho SJ, Magennis EM, Singh CK, Kelly BT. Outcomes after the arthroscopic treatment of femoroacetabular impingement in a mixed group of high-level athletes. The American journal of sports medicine. 2011;39 Suppl:14S-9S. Epub 2011/07/08.
42. Beaulé PE, Le Duff MJ, Zaragoza E. Quality of life following femoral head-neck osteochondroplasty for femoroacetabular impingement. The Journal of Bone & Joint Surgery. 2007;89(4):773-9.
43. Southwick WO. Osteotomy through the lesser trochanter for slipped capital femoral epiphysis. The Journal of Bone & Joint Surgery. 1967;49(5):807-35.
44. Kasa I. A circle fitting procedure and its error analysis. Instrumentation and Measurement, IEEE Transactions on. 1976;1001(1):8-14.
45. Murphy MJ. The importance of computed tomography slice thickness in radiographic patient positioning for radiosurgery. Medical Physics. 1999;26:171.
46. Berteau JP, Pithioux M, Baron C, Gineyts E, Follet H, Lasaygues P, et al. Characterisation of the difference in fracture mechanics between children and adult cortical bone. Computer methods in biomechanics and biomedical engineering. 2012;15(sup1):281-2.
47. Bergmann G, Deuretzbacher G, Heller M, Graichen F, Rohlmann A, Strauss J, et al. Hip contact forces and gait patterns from routine activities. Journal of Biomechanics. 2001;34(7):859-71.
48. Polgar K, Viceconti M, Connor J. A comparison between automatically generated linear and parabolic tetrahedra when used to mesh a human femur. Proceedings of the Institution of Mechanical Engineers, Part H: Journal of Engineering in Medicine. 2001;215(1):85-94.
49. Yosibash Z, Trabelsi N, Milgrom C. Reliable simulations of the human proximal femur by high-order finite element analysis validated by experimental observations. Journal of Biomechanics. 2007;40(16):3688-99.
50. Öhman C, Baleani M, Pani C, Taddei F, Alberghini M, Viceconti M, et al. Compressive behaviour of child and adult cortical bone. Bone. 2011;49(4):769-76.
51. Eberle S, Göttlinger M, Augat P. An investigation to determine if a single validated density–elasticity relationship can be used for subject specific finite element analyses of human long bones. Medical Engineering & Physics. 2012.
52. Helgason B, Perilli E, Schileo E, Taddei F, Brynjólfsson S, Viceconti M. Mathematical relationships between bone density and mechanical properties: a literature review. Clinical Biomechanics. 2008;23(2):135-46.
53. Taddei F, Viceconti M, Manfrini M, Toni A. Mechanical strength of a femoral reconstruction in paediatric oncology: a finite element study. Proceedings of the Institution of Mechanical Engineers, Part H: Journal of Engineering in Medicine. 2003;217(2):111-9.
54. Fishkin Z, Armstrong DG, Shah H, Patra A, Mihalko WM. Proximal femoral physis shear in slipped capital femoral epiphysis-a finite element study. Journal of Pediatric Orthopaedics. 2006;26(3):291-4.
55. Carter DR, Wong M. The role of mechanical loading histories in the development of diarthrodial joints. Journal of Orthopaedic Research. 2005;6(6):804-16.
56. Taddei F, Martelli S, Reggiani B, Cristofolini L, Viceconti M. Finite-element modeling of bones from CT data: sensitivity to geometry and material uncertainties. Biomedical Engineering, IEEE Transactions on. 2006;53(11):2194-200.
57. Peng L, Bai J, Zeng X, Zhou Y. Comparison of isotropic and orthotropic material property assignments on femoral finite element models under two loading conditions. Medical Engineering & Physics. 2006;28(3):227-33.

58. Baca V, Horak Z, Mikulenka P, Dzupa V. Comparison of an inhomogeneous orthotropic and isotropic material models used for FE analyses. Medical Engineering & Physics. 2008;30(7):924-30.
59. Macirowski T, Tepic S, Mann RW. Cartilage stresses in the human hip joint. Journal of biomechanical engineering. 1994;116(1):10.
60. Carriero A, Zavatsky A, Stebbins J, Theologis T, Lenaerts G, Jonkers I, et al. Influence of altered gait patterns on the hip joint contact forces. Computer Methods in Biomechanics and Biomedical Engineering. 2012(ahead-of-print):1-8.
61. Bergmann GeCU. OrthoLoad, Loading of Orthopaedic Implants. 2008 medizin Berlin.
62. Carter D, Orr T, Fyhrie D. Relationships between loading history and femoral cancellous bone architecture. Journal of Biomechanics. 1989;22(3):231-44.
63. Bergmann G, Graichen F, Rohlmann A. Hip joint loading during walking and running, measured in two patients. Journal of Biomechanics. 1993;26(8):969-90.
64. Cleather DJ, Goodwin JE, Bull AM. Hip and knee joint loading during vertical jumping and push jerking. Clinical Biomechanics. 2012.
65. Shefelbine SJ, Carter DR. Mechanobiological predictions of growth front morphology in developmental hip dysplasia. Journal of Orthopaedic Research. 2004;22(2):346-52.
66. Lin H, Aubin CÉ, Parent S, Villemure I. Mechanobiological bone Growth: Comparative analysis of two biomechanical modeling approaches. Medical and Biological Engineering and Computing. 2009;47(4):357-66.
67. Villemure I, Stokes IAF. Growth plate mechanics and mechanobiology. A survey of present understanding. Journal of Biomechanics. 2009;42(12):1793-803.
68. Stokes IA, Laible JP. Three-dimensional osseo-ligamentous model of the thorax representing initiation of scoliosis by asymmetric growth. J Biomech. 1990;23(6):589-95.
69. Carter DR, Wong M. Mechanical stresses and endochondral ossification in the chondroepiphysis. J Orthop Res. 1988;6(1):148-54.
70. Carter DR, Beaupré GS. Skeletal function and form: mechanobiology of skeletal development, aging, and regeneration: Cambridge University Press; 2007.
71. Carter DR, Orr TE, Fyhrie DP, Schurman DJ. Influences of mechanical stress on prenatal and postnatal skeletal development. Clinical orthopaedics and related research. 1987;219:237.
72. Matsuda JJ, Zernicke RF, Vailas AC, Pedrini VA, Pedrini-Mille A, Maynard JA. Structural and mechanical adaptation of immature bone to strenuous exercise. Journal of Applied Physiology. 1986;60(6):2028-34.
73. Carriero A, Jonkers I, Shefelbine SJ. Mechanobiological prediction of proximal femoral deformities in children with cerebral palsy. Computer methods in biomechanics and biomedical engineering. 2011;14(03):253-62.
74. Shefelbine SJ, Carter DR. Mechanobiological predictions of femoral anteversion in cerebral palsy. Annals of Biomedical Engineering. 2004;32(2):297-305.
75. Kienle KP. Femoral Morphology and Epiphyseal Growth Plate Changes of the Hip During Maturation: MR Assessments in a One Year Follow Up on a Cross Sectional Asymptomatic Cohort in the Age Range 9 - 17 Years2012.
76. Ogden. Anatomy and Physiology of Skeletal Development.
77. Kandzierski G, Matuszewski Ł, Wójcik A. Shape of growth plate of proximal femur in children and its significance in the aetiology of slipped capital femoral epiphysis. International orthopaedics. 2012;36(12):2513-20.
78. Piszczatowski S. Geometrical aspects of growth plate modelling using Carter's and Stokes's approaches. Acta of bioengineering and biomechanics/Wrocław University of Technology. 2012;14(1):93.
79. Mirtz TA, Chandler JP, Eyers CM. The effects of physical activity on the epiphyseal growth plates: A review of the literature on normal physiology and clinical implications. Journal of clinical medicine research. 2011;3(1):1.
80. Siebenrock K, Behning A, Mamisch T, Schwab J. Growth Plate Alteration Precedes Cam-type Deformity in Elite Basketball Players. Clinical orthopaedics and related research. 2012.

81. Wong M, Carter DR. A theoretical model of endochondral ossification and bone architectural construction in long bone ontogeny. Anatomy and embryology. 1990;181(6):523-32.
82. Ribble TG, Santare M, Miller F. Stresses in the growth plate of the developing proximal femur. Journal of Applied Biomechanics. 2001;17(2):129-41.
83. Brown T, Way M, Fu F, Ferguson Jr A. Load transmission through the proximal femur of the growing child: a finite element analysis. Growth. 1980;44(4):301.
84. Ueki M, Tanaka N, Tanimoto K, Nishio C, Honda K, Lin Y-Y, et al. The effect of mechanical loading on the metabolism of growth plate chondrocytes. Annals of biomedical engineering. 2008;36(5):793-800.
85. Wong M, Wuethrich P, Buschmann M, Eggli P, Hunziker E. Chondrocyte biosynthesis correlates with local tissue strain in statically compressed adult articular cartilage. Journal of Orthopaedic Research. 1997;15(2):189-96.
86. Chung S, Batterman S, Brighton C. Shear strength of the human femoral capital epiphyseal plate. The Journal of bone and joint surgery American volume. 1976;58(1):94.
87. Williams JL, Do PD, David Eick J, Schmidt TL. Tensile properties of the physis vary with anatomic location, thickness, strain rate and age. Journal of Orthopaedic Research. 2001;19(6):1043-8.
88. Zupanc O, Križancic M, Daniel M, Mavcic B, Antolic V, Iglic A, et al. Shear stress in epiphyseal growth plate is a risk factor for slipped capital femoral epiphysis. Journal of Pediatric Orthopaedics. 2008;28(4):444-51.
89. Modenese L, Phillips A, Bull A. An open source lower limb model: Hip joint validation. Journal of Biomechanics. 2011;44(12):2185-93.
90. Wille H, Rank E, Yosibash Z. Prediction of the mechanical response of the femur with uncertain elastic properties. Journal of Biomechanics. 2012.
91. Hymer WC, Kraemer WJ, Nindl BC, Marx JO, Benson DE, Welsch JR, et al. Characteristics of circulating growth hormone in women after acute heavy resistance exercise. American Journal of Physiology-Endocrinology And Metabolism. 2001;281(4):E878-E87.
92. Steenbekkers L. Child development, design implications and accident prevention. 1993.
93. Rissech C, Schaefer M, Malgosa A. Development of the femur—implications for age and sex determination. Forensic science international. 2008;180(1):1-9.
94. Isaac B, Vettivel S, Prasad R, Jeyaseelan L, Chandi G. Prediction of the femoral neck-shaft angle from the length of the femoral neck. Clinical Anatomy. 1997;10(5):318-23.

Appendix 1

Subject	949141	Mean Values
Gender	Male	Male
Age (years)	12	12
Length (cm)	167.7	156.3 (92)
Weight (kg)	48	42 (92)
Affected leg	left	X
Femoral head diameter (mm)	42.2	35.2 (93)
Alpha angle (°)	40.1	<60 (no Cam) (17)
Neck/shaft angle (°)	133.2	140 (94)

Subject information of CT data set.

Appendix 2

Maximum edge length (Mimics)	7	5	4	3	2.5	2	1.75	1.5
Mean edge length (Abaqus) (mm)	3.66	3.01	2.49	1.90	1.59	1.27	1.11	0.93
Volume Model (mm^3)	102018	102017	102032	102048	102055	102066	102070	102076
Number of elements	17627	31911	55868	126212	215616	421064	630767	1064066
Number of nodes (linear)	4266	6570	10468	22176	36952	70584	104830	165782
nDOF (linear)	12468	19266	30909	65967	110229	210849	313329	495867
Number of nodes (quadratic)	28897	47940	80004	175073	295467	571111	X	X
nDOF (quadratic)	85308	141789	238434	523332	882273	1710381	X	X

The mean edge length in Abaqus is calculated using the volume-edge length function for a tetrahedron: $V = a^3/6\sqrt{2}$. *He total volume of the model is divided by the number of elements to get the mean volume of one element. The degrees of freedom (NDOF) is the number of nodes that are not confined times 3.*

Appendix 3

Import DICOM images	
Compression	CT
Thresholding	Bone (CT) min:226 max:2148
Laplacian (1st order)	
Smooth factor	1
Number of iterations	3
Reduce parameters	
Flip threshold angle	30.0
Geometrical error	0.1
Number of iterations	5
Auto-Remesh/Reduce number of triangles	
Shape Quality threshold	0.4
Maximum geometrical error	0.2
Maximal edge length	1.5
Number of iterations	3
Create volume mesh	
Method	Init and Refine
Maximum edge length	1.5
Shape measure	Aspect ratio (A)
Shape quality threshold	25.0

Segmentation and meshing parameters.

Appendix 4

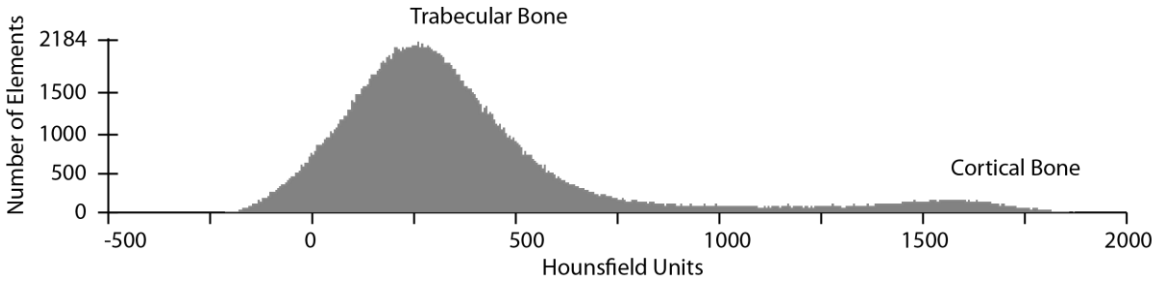

Histogram of the distribution of the HU values and consequently the material. Showing a large trabecular and a small cortical bone peak.

Appendix 5

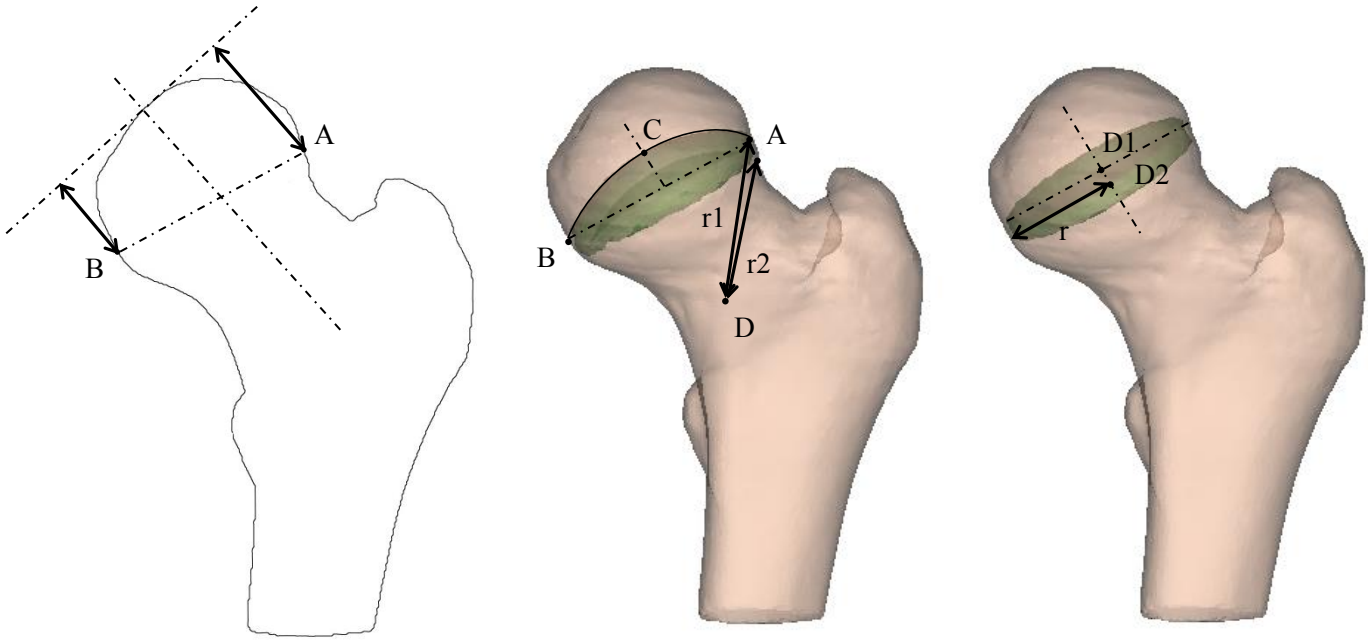

a) **b)** **c)**

Determination of the Growth Plate orientation. (a) Cross-section of the femur to determine the superior and inferior extension of the growth plate. A and B are based on the calculated epiphyseal extension Q1 and Q2 of the medical image analysis. (b) Point C determines the convexity of the growth plate and is chosen based on visual analysis of the scans. The convex growth plate is segmented using a sphere with midpoint D with an upper and lower boundary (r1 and r2). (c) The flat growth plates were modeled using two cylinders with midpoints D1 and D2 with the same orientation as the convex plate.

Appendix 6

		x	y	z	Radius	Length
Sphere (Convex)	GP1	91.171432	-80.966443	-1394.352351	33 & 30	
	GP2	89.775984	-82.700113	-1396.726474	32 & 29	
	GP3	88.728083	-84.015935	-1399.905797	32 & 29	
Cylinder (Flat)	GP1	80.645357	-92.609444	-1369.864894	20	3.18
		81.893101	-91.22905	-1372.755005		
	GP2	81.23318	-91.708407	-1371.734298	20	3.45
		82.278103	-90.577049	-1374.823303		
	GP3	81.866444	-90.770424	-1373.648382	20	3.41
		82.68	-89.921249	-1376.848877		
Bottom shaft		96.0427	-75.1996	-1454.5970		
Center of the neck		90.0497	-81.1955	-1384.9380		
Center femoral head		82.9889	-90.5428	1371.8536		

Coordinates of the center of the spheres and cylinders and the radii of GP1, GP2 and GP3. In addition, the coordinates of some reference points of the model.

Appendix 7

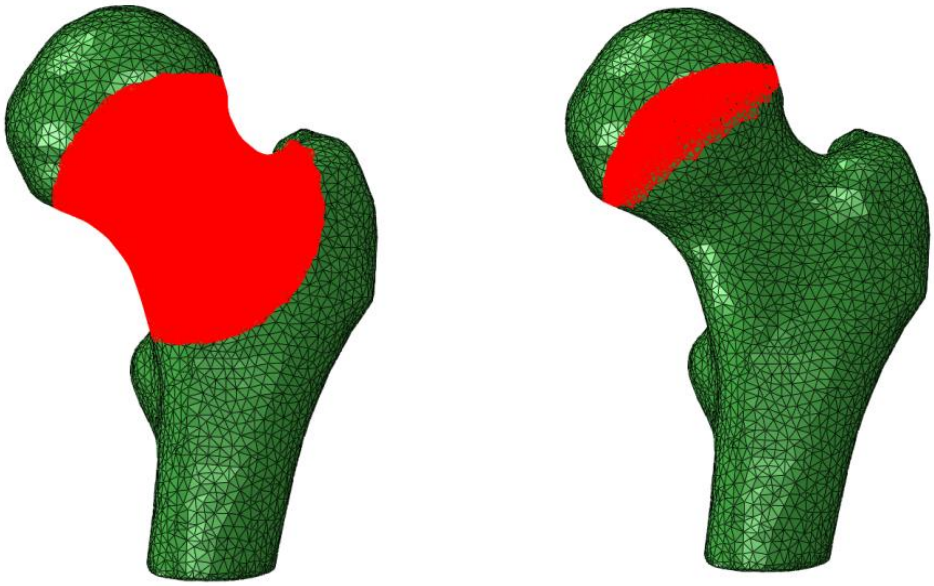

a) **b)**

Segmentation Protocol of the growth plate in Abaqus. (a) A set represents the elements where the femur intersects with the sphere. (b) By subtracting two spheres with the same origin and different radius, the convex growth plate is segmented.

Appendix 8

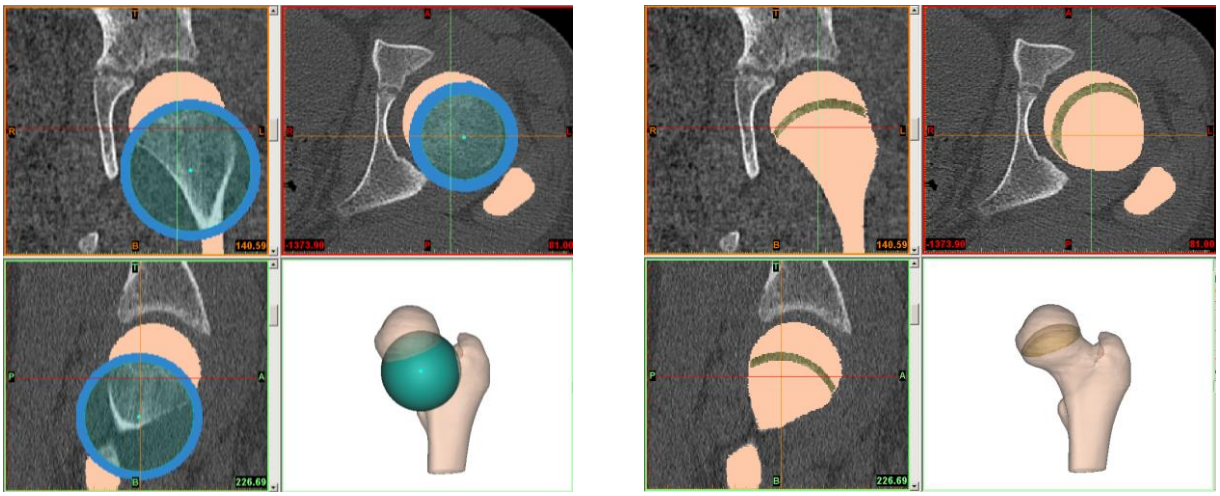

a) **b)**

Segmentation Protocol of the growth plate in Mimics. (a) Two spherical masks are calculated from the CAD objects, which can be seen in a top, sagittal and anteroposterior (AP) view. (b) After morphological and Boolean operations the surface mask of the growth plate is calculated.

Appendix 9

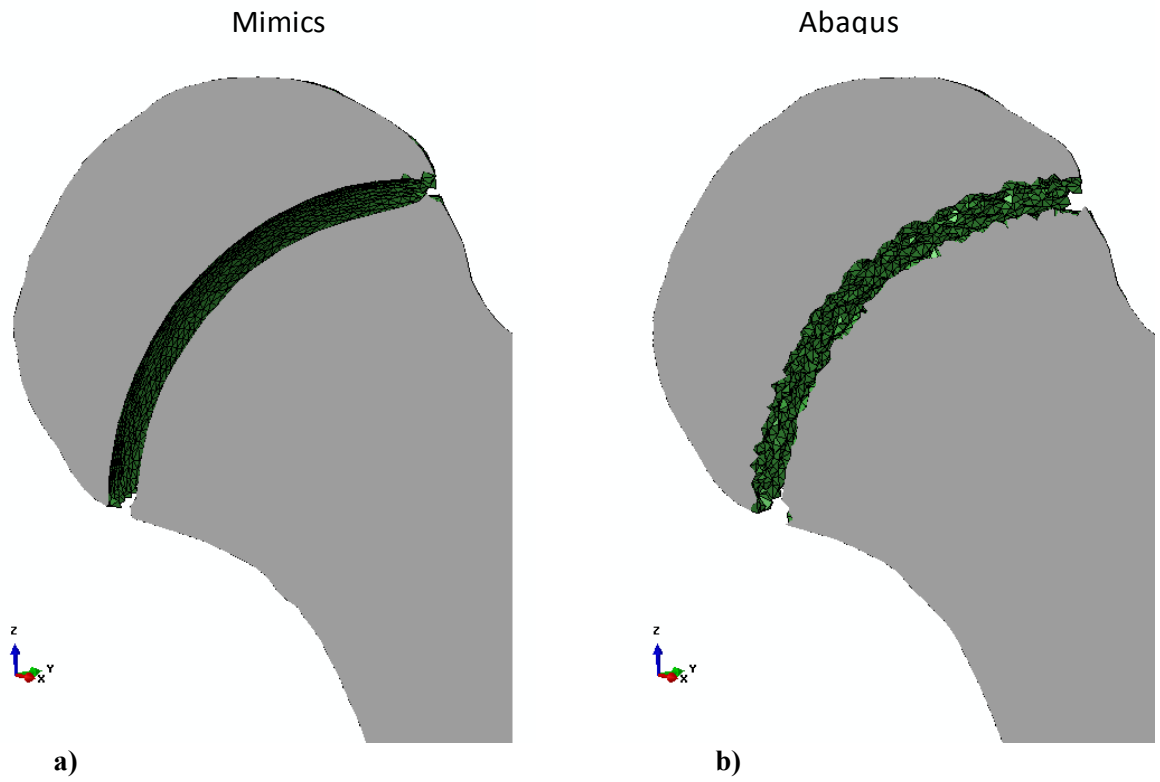

Cross sectional view illustrating the segmentation in (a) Mimics (smooth surface) and (b) Abaqus (rough surface).

Appendix 10

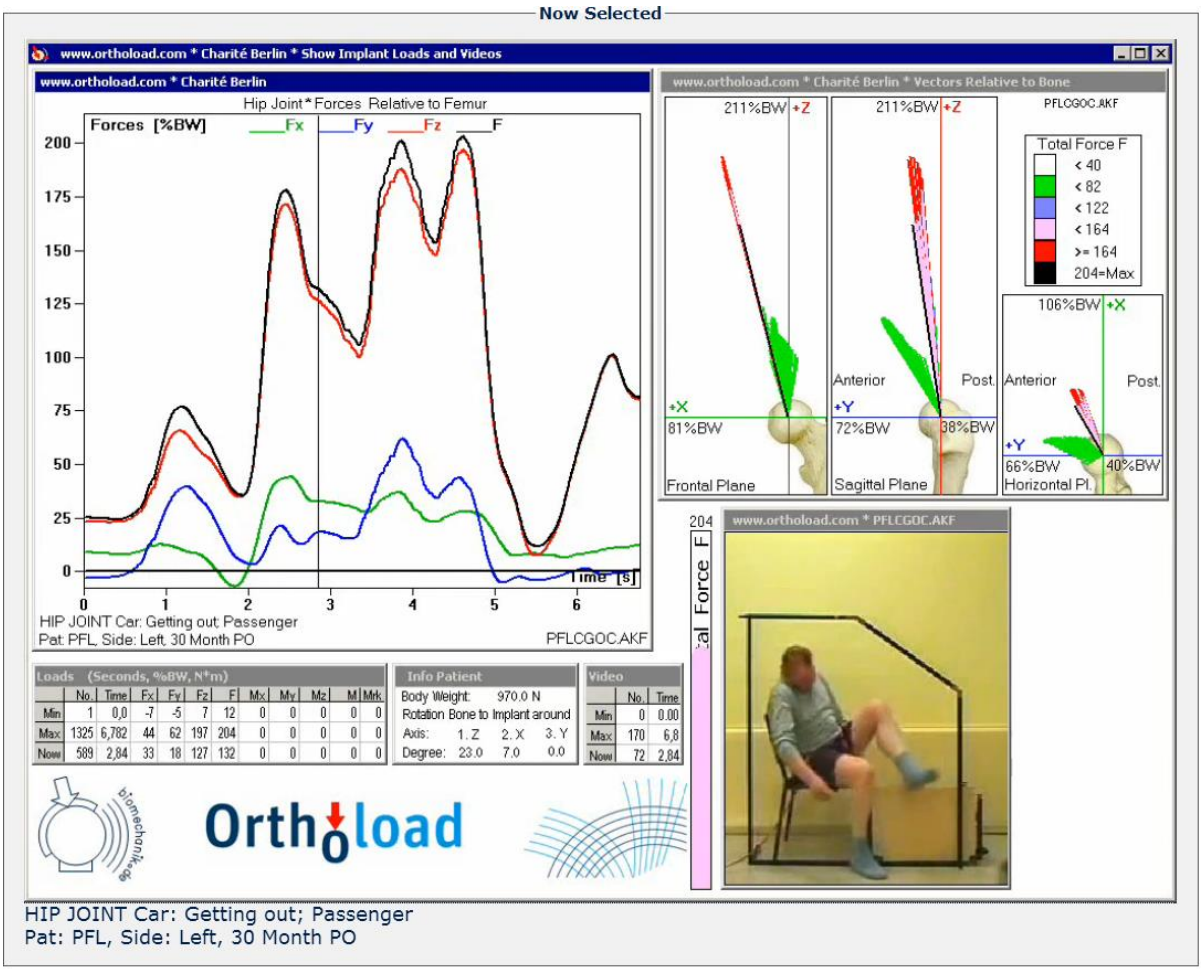

Data of implant loads and videos from the database of OrthoLoad (61) for the movement: Passenger getting out of a car. Left: Hip Joint Force vectors relative to the femur in %BW. Right: Coronal, Sagittal and Transverse plane showing the direction force vector.

Appendix 11

	Forces on the Femoral Head				Muscle Force	
Model	Coronal Medial (deg)	Transverse Ventral (deg)	Sagittal Anterior (deg)	Magnitude (N)	Coronal Medial (deg)	Magnitude (N)
Normal gait	13	31	22	-	-	-
Case 1	15	35	20	1200	-	-
Internal rotation	33	13	9	-	-	-
Case 2	40	15	10	1200	35	364
Case 3	-15	90	10	1200	-8	364
Hip flexion	15	80	45	-	-	-
Case 4	15	80	70	1200	-	-

Comparison of loading conditions of the proximal femur in previous studies (47, 60, 61). The inclination angles are positive in lateral or posterior direction.

Appendix 12

	HH=1	HH=2	HH=3	1 vs. 3 p-value	AA < 60	AA > 60	p-value
Q1	1.39	1.53	1.69	**0.047**	1.43	1.54	**0.001**
Q2	0.82	0.86	0.97	0.056	0.84	0.86	0.845
Tilt Angle	18.08	20.39	21.74	0.545	18.5	20.8	**0.024**
Neck-Shaft Angle	132.7	130.92	132.9	0.936	133.61	129.12	**0.001**
Mean AA	52.16	58.48	69.34				

	Open growth plate			**Closed growth plate**		
	no cam (n=63)	cam (n=33)	p-value	no cam (n=17)	cam (n=13)	p-value
Q1	1.39	1.48	**0.013**	1.59	1.68	**0.028**
Q2	0.84	0.84	0.474	0.85	0.91	0.77
Tilt Angle	17.27	19.76	**0.012**	22.97	23.28	0.4
Neck-Shaft Angle	134.24	128.48	**0.000**	131.28	130.8	0.28

Mean Values of the Neck-Shaft angle, Tilt angle, Q1 and Q2 defined by Highest Hip (HH) Score and Alpha Angle (AA). Cam and no Cam for the open and closed group are defined by the alpha angle.

HH : A three point scoring system, where 1 indicates a normal joint, 2, a flattening of the head-neck junction and 3 a prominence bump (17).

AA : The angle between the neck axis and the line from the center of the femoral head through the point where the cortical surface exceeds the radius of a perfect circle drawn around an ideally spherical femoral head. α *>60, indicates a Cam.*

Appendix 13

Osteogenic Index

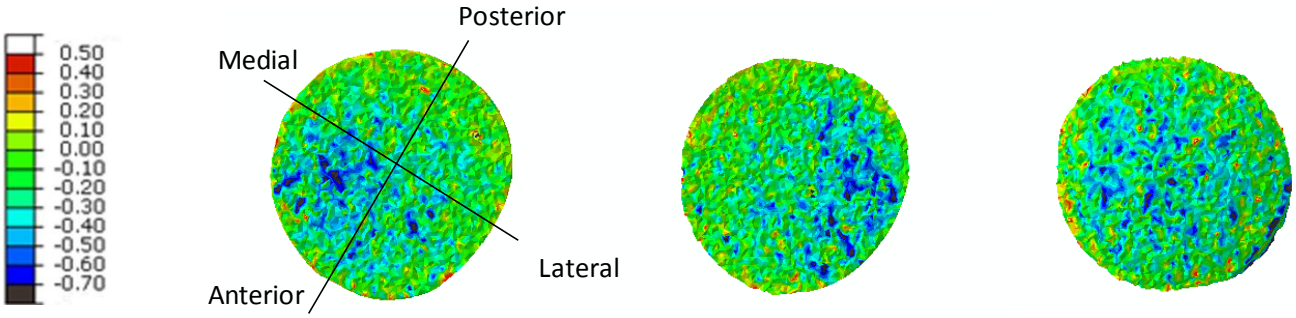

Osteogenic Index distribution in (a) GP 3 higher in head, (b) GP3 flat and (C) GP3 convex under loading condition 2.

Appendix 14

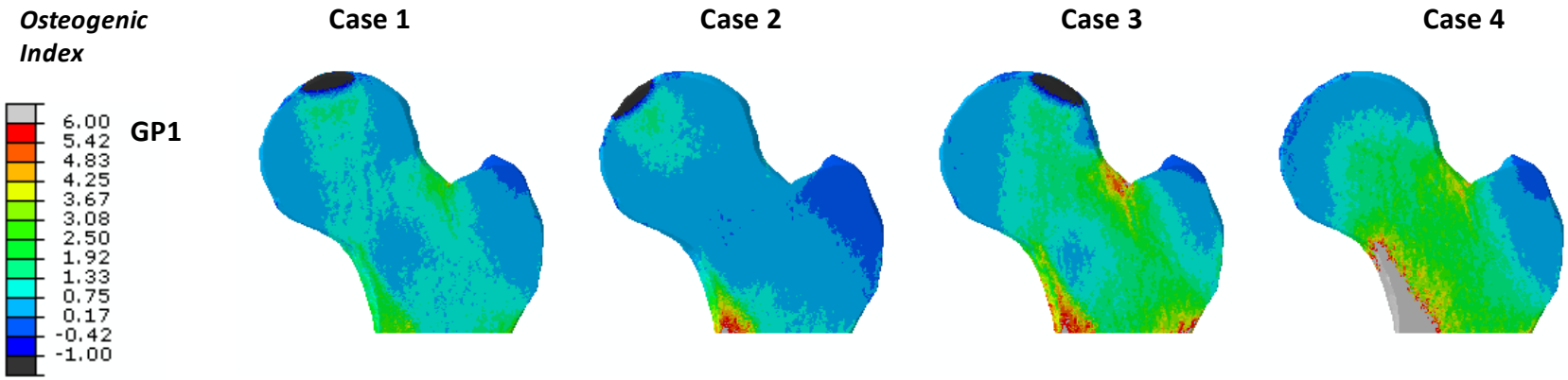

Osteogenic Index (OI) distribution of the proximal femur under four loading conditions. Without modeling of a growth plate.

Appendix 15

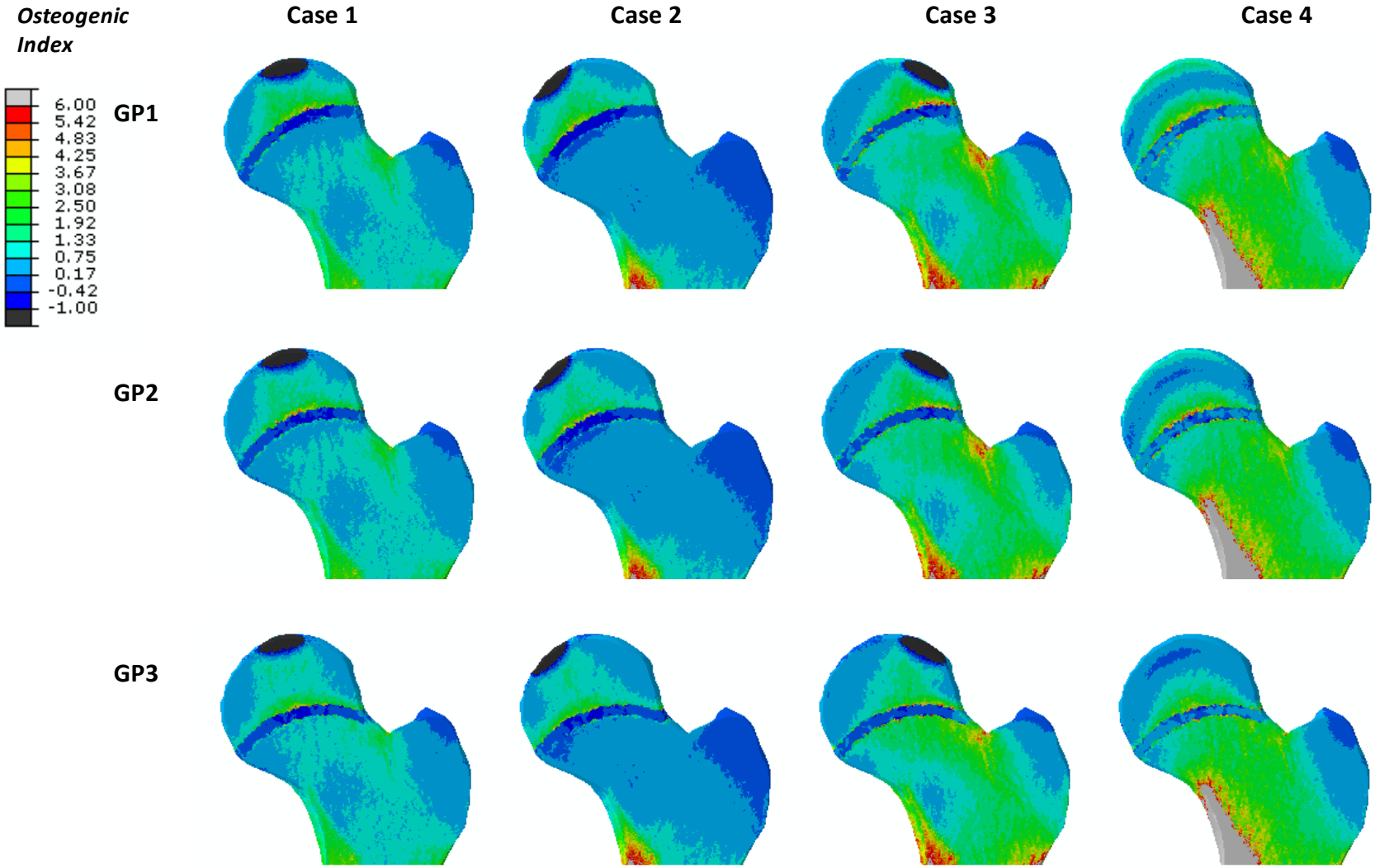

Osteogenic Index (OI) distribution of the proximal femur under four loading conditions. Growth plate modeled as a convex disk in Abaqus.

Appendix 16

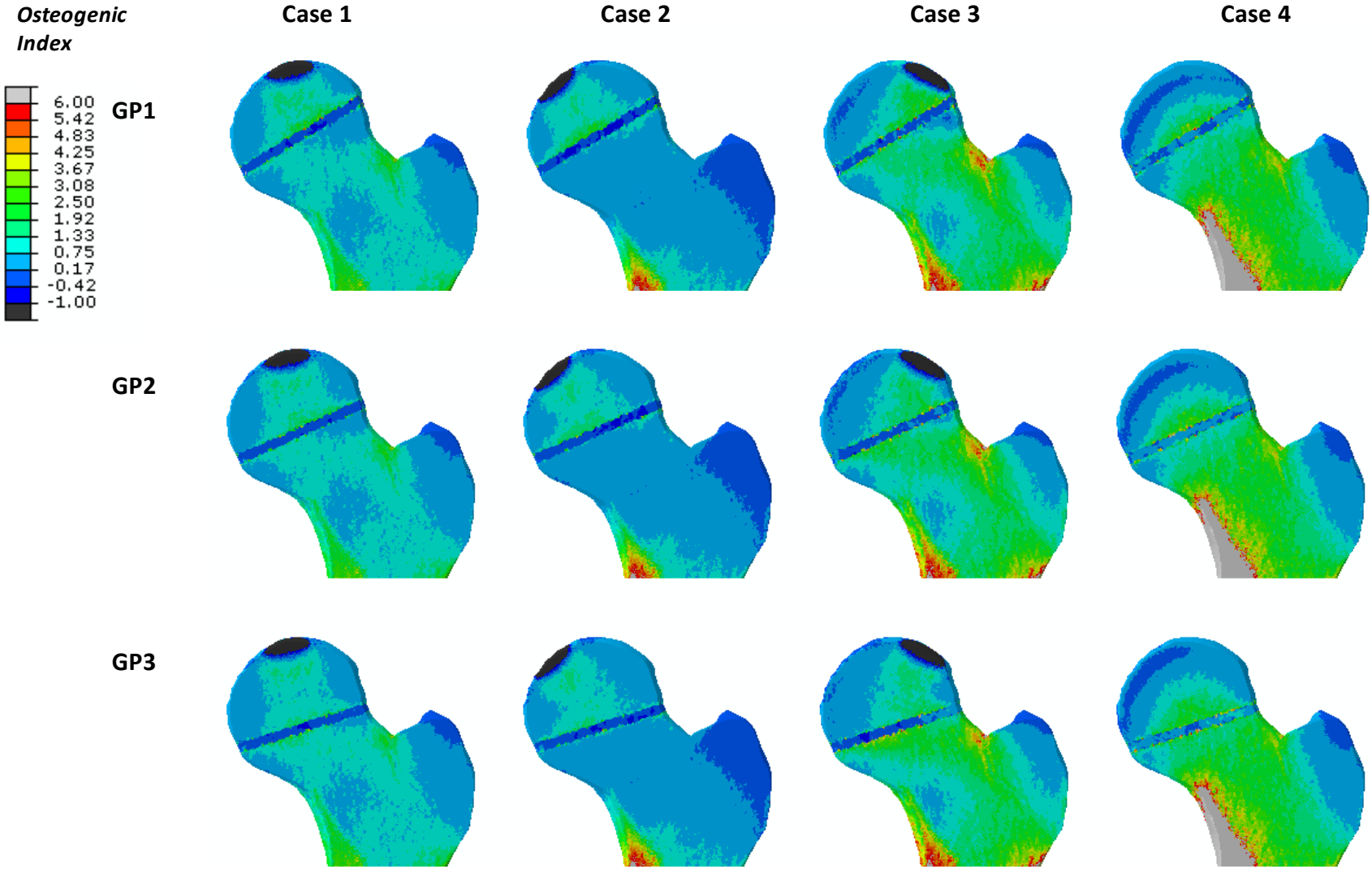

Osteogenic Index (OI) distribution of the proximal femur under four loading conditions. Growth plate modeled as a flat disk in Abaqus.

Appendix 17

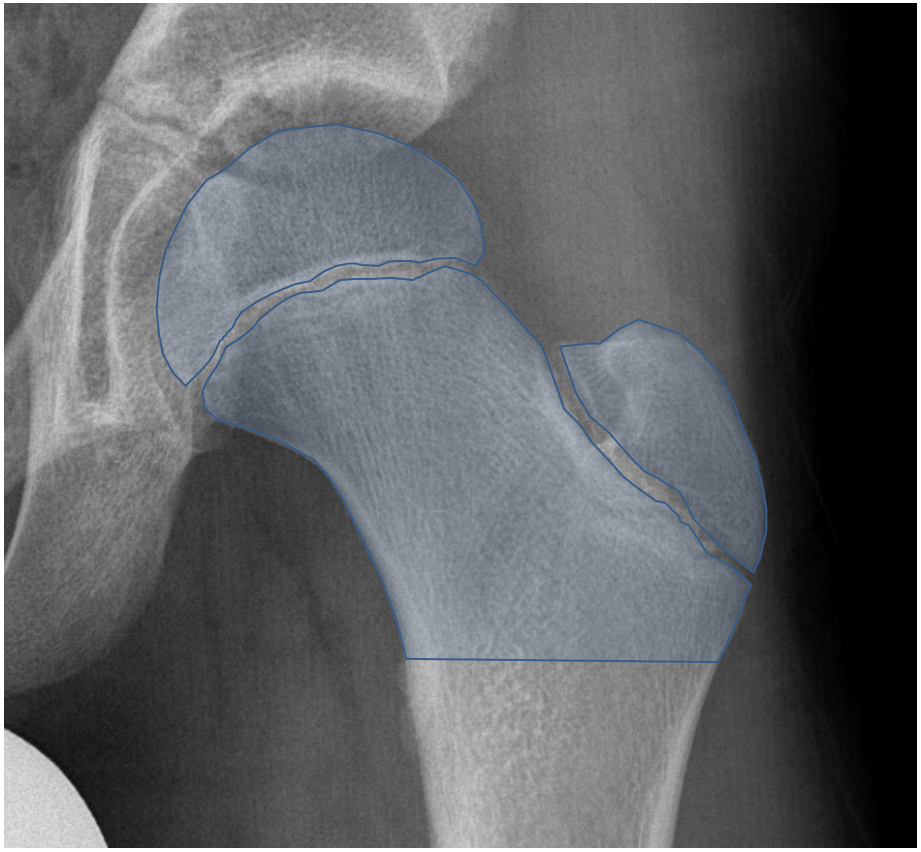

a)

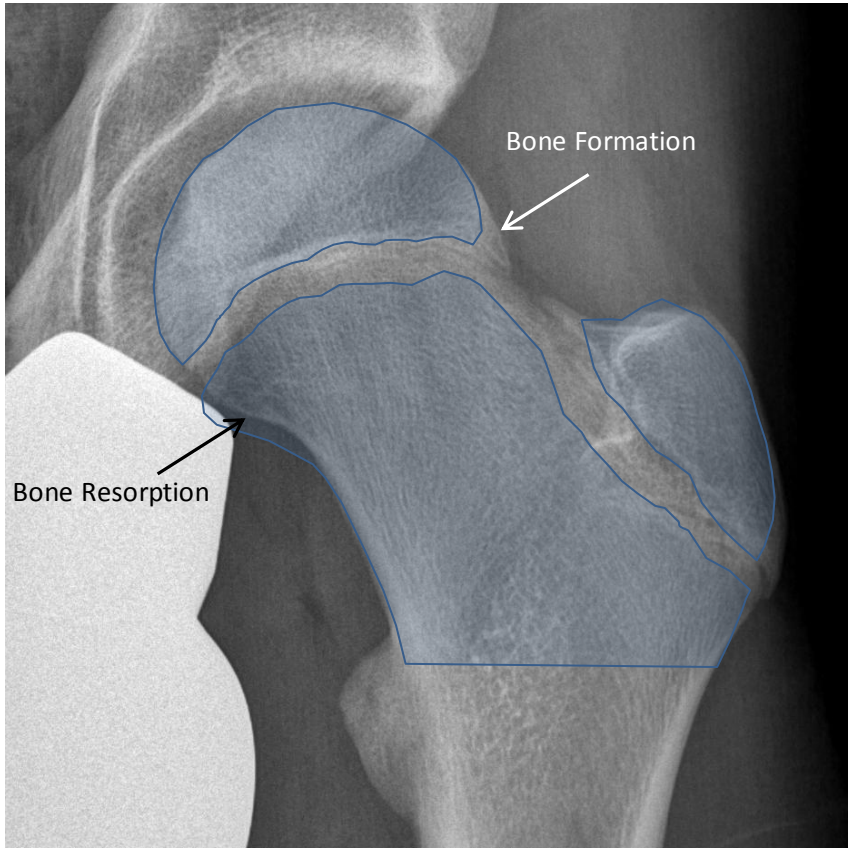

b)

(a) Radiograph of a femur with an epiphyseal extension of Q1>1.4 at baseline and (b) the same femur at 2 year follow-up with alpha angle>60°. The blue contour indicates the shape and illustrate the growth region.